

Finite element and isogeometric stabilized methods for the advection-diffusion-reaction equation

Citation for published version (APA):

Key, K., Abdelmalik, M. R. A., Elgeti, S., Hughes, T. J. R., & Baidoo, F. A. (2023). Finite element and isogeometric stabilized methods for the advection-diffusion-reaction equation. *Computer Methods in Applied Mechanics and Engineering*, 417(Part B.), Article 116354. <https://doi.org/10.1016/j.cma.2023.116354>

Document license:

CC BY

DOI:

[10.1016/j.cma.2023.116354](https://doi.org/10.1016/j.cma.2023.116354)

Document status and date:

Published: 15/12/2023

Document Version:

Publisher's PDF, also known as Version of Record (includes final page, issue and volume numbers)

Please check the document version of this publication:

- A submitted manuscript is the version of the article upon submission and before peer-review. There can be important differences between the submitted version and the official published version of record. People interested in the research are advised to contact the author for the final version of the publication, or visit the DOI to the publisher's website.
- The final author version and the galley proof are versions of the publication after peer review.
- The final published version features the final layout of the paper including the volume, issue and page numbers.

[Link to publication](#)

General rights

Copyright and moral rights for the publications made accessible in the public portal are retained by the authors and/or other copyright owners and it is a condition of accessing publications that users recognise and abide by the legal requirements associated with these rights.

- Users may download and print one copy of any publication from the public portal for the purpose of private study or research.
- You may not further distribute the material or use it for any profit-making activity or commercial gain
- You may freely distribute the URL identifying the publication in the public portal.

If the publication is distributed under the terms of Article 25fa of the Dutch Copyright Act, indicated by the "Taverne" license above, please follow below link for the End User Agreement:

www.tue.nl/taverne

Take down policy

If you believe that this document breaches copyright please contact us at:

openaccess@tue.nl

providing details and we will investigate your claim.



Finite element and isogeometric stabilized methods for the advection-diffusion-reaction equation

Konstantin Key^{d,a}, Michael R.A. Abdelmalik^{b,*}, Stefanie Elgeti^{a,d}, Thomas J.R. Hughes^c,
Frimpong A. Baidoo^c

^a Institute for Lightweight Design and Structural Biomechanics, TU Wien, Austria

^b Department of Mechanical Engineering, Eindhoven University of Technology, Netherlands

^c Computational Mechanics Group, Oden Institute, UT Austin, United States of America

^d Chair for Computational Analysis of Technical Systems, RWTH Aachen University, Germany

Available online 2 September 2023

Abstract

We develop two new stabilized methods for the steady advection-diffusion-reaction equation, referred to as the **Streamline GSC Method** and the **Directional GSC Method**. Both are globally conservative and perform well in numerical studies utilizing linear, quadratic, cubic, and quartic Lagrange finite elements and maximally smooth B-spline elements. For the streamline GSC method we can prove coercivity, convergence, and optimal-order error estimates in a strong norm that are robust in the advective and reactive limits. The directional GSC method is designed to accurately resolve boundary layers for flows that impinge upon the boundary at an angle, a long-standing problem. The directional GSC method performs better than the streamline GSC method in the numerical studies, but it is not coercive. We conjecture it is *inf-sup* stable but we are unable to prove it at this time. However, calculations of the *inf-sup* constant support the conjecture. In the numerical studies, B-spline finite elements consistently perform better than Lagrange finite elements of the same order and number of unknowns.

© 2023 The Author(s). Published by Elsevier B.V. This is an open access article under the CC BY license (<http://creativecommons.org/licenses/by/4.0/>).

Keywords: Advection; Diffusion; Reaction; Stabilized methods; Finite element method; Isogeometric analysis

1. Introduction

The linear, steady ADR equation is ostensibly a very simple partial differential equation, but it has numerous important physical applications and is also an important model equation for the study of nonlinear and more complex flow phenomena. However, its stable and accurate numerical solution has, somewhat surprisingly, proven to be a challenge. The two limiting cases of AD and RD are much simpler, and there are effective methods for both, but the full ADR equation represents a significant increase in difficulty. The study of stabilized methods for the ADR equation began with [Harari and Hughes \[1\]](#). This study was confined to one dimension but it was discovered that there would need to be two stabilizing mechanisms, and two accompanying parameters to be determined. It was a step forward but indicated that the accurate numerical formulation of the ADR equation was more complicated than previously thought. The instabilities noted in Galerkin methods for advection were stronger than those produced

* Corresponding author.

E-mail address: m.abdel.malik@tue.nl (M.R.A. Abdelmalik).

by reaction, but controlling the interaction of advection and reaction was a much more complicated problem. [1] was followed over the years by a number of studies that sought better solutions to the problem [2–17]. A complete review of the history of this topic is presented in Hauke–Sangalli–Doweidar [18], who also produced a Variational-Multiscale-inspired stabilized method that produced both good quality numerical results and was amenable to a complete mathematical stability and convergence analysis, and resulting error estimates. This is the best and most complete work to date. However, everything was restricted to linear elements.

This paper presents and analyses a new class of finite element and isogeometric stabilized methods for the ADR equation. We refer to these as **GSC methods**. (We apologize for all the acronyms and hope the reader will patiently bear with us.) We begin with a study of the homogeneous, one-dimensional case assuming continuous, piecewise linear, finite elements, which may be viewed alternatively as the first member of the Lagrange family of finite elements or as the first member of the family of maximally smooth B-spline elements. For this case, it is well known that a stabilized method must have at least two stabilization parameters associated with the two exact solutions of the ADR equation. We note that for the two limiting cases, AD and RD, only one stabilization parameter is required. The two stabilization parameters are denoted τ_A and τ_R and are associated with weighting by the advection operator and reaction operator, respectively. The idea is seen to be similar to methods referred to as GLS/GGLS, that is Galerkin Least-Squares/Galerkin Gradient Least-Squares [10]. However, GSC methods are a combination of standard SUPG for advection and the gradient of the residual weighted by the gradient of the reaction term. The advantage of this is that the same global conservation law¹ as that for the exact ADR equation, and also the Galerkin method, is obtained for GSC methods. Conservation is often viewed as a test for a well-formulated numerical method. We note that [10] and the more recent method of Hauke-Sangalli-Doweidar [18] do not satisfy this conservation law. With the GSC formulation we are able to identify stabilization parameters τ_A and τ_R such that the methods are nodally exact for the linear finite element model problem. This, in itself, is not a unique accomplishment as previous methods have obtained this attribute.

We then study the behavior of the GSC method for linear, quadratic, cubic, and quartic Lagrange and B-spline finite elements on AD, RD, and ADR model problems *using the exact same stabilization parameters τ_A and τ_R obtained for the linear element case*. There is some evidence that stabilization parameters for higher-order elements are not substantially different than those for linear elements (see Hughes and Sangalli [19]). However, this topic warrants further study. In comparing these methods, we set the number of degrees of freedom to be the same for all calculations, resulting in element lengths being different in each case. Comparison is also made to the Galerkin method. In addition, we performed convergence rate studies and found that optimal convergence rates are obtained in H^1 for all cases. However, we observed two deficiencies. One is numerical sensitivity. We found in a Mathematica implementation of the parameter formulas that inaccurate results were obtained in certain circumstances. We attribute this problem to expressions in the denominators of the formulas, which involve differences of hyperbolic functions taking nearly the same large values, leading to significant errors in the differences. The second deficiency concerned L^2 convergence rates, which were not always optimal. Consequently, we developed alternative, approximate stabilization parameters that corrected both deficiencies. The suite of one-dimensional problems was repeated for the approximate stabilization parameters. We note that the approximate stabilization parameters no longer obtain the nodally exact solutions for linear finite elements, but performed quite well for all cases. They are also more efficient, eliminating all hyperbolic functions. We use the approximate formulas in place of the exact throughout the remainder of the paper.

We present two GSC methods for multidimensions that generalize the one-dimensional method. The first, referred to as the **Streamline GSC Method**, employs the streamline operator as in SUPG. The advective stabilization parameter τ_A follows the usual generalization to multidimensions in which the advective velocity in one-dimension is replaced by the Euclidean norm of the advective velocity. The reactive stabilization parameter τ_R is the same as in one dimension. We begin our study of this method with numerical calculations of AD, RD, and ADR two-dimensional problems that have sharp boundary layers. As in the one-dimensional case, the B-spline elements outperform the Lagrange elements on meshes that have an equal number of degrees of freedom.

We then proceed to perform a complete stability and convergence analysis of the streamline GSC method that is applicable to multidimensional and higher-order cases. We show that the method is coercive in a strong norm, the

¹ The conservation law in question emanates from the weak form when we assume Neumann boundary conditions and set the weighting function to a constant. All stabilization terms in GSC methods vanish in these cases and the variational equation reduces to the Galerkin method.

GSC norm, and achieves optimal error estimates in it. Furthermore, the convergence is robust in that it is uniform under conditions of advection and reaction dominance. We believe this is the first full functional analysis proof for higher-order elements and B-spline elements of a stabilized method for the ADR equation.

The second method is referred to as the **Directional GSC Method**. This method was devised to address a problem associated with sharp boundary layers when the flow is at an angle to the boundary. It has been repeatedly noted in the literature that the SUPG method produces a substantial overshoot in this case for linear elements. At the same time, if the flow is normal to the boundary, SUPG produces nodally exact results. We wished to preserve this property when the flow was at an angle to the boundary. Our analysis revealed that the way to do this was to decompose the advection and reaction weighting into two one-dimensional terms, each with its own stabilization parameters τ_A and τ_R computed from the one-dimensional formula with the advective velocity component corresponding to the flow in the principal directions of the element. We were not sure that this method would achieve the same accuracy as the streamline GSC method but we were gratified to find that the results for the two-dimensional problems previously considered were actually better. We were still concerned that these problems, which featured uniform velocity fields skew to the mesh, did not provide sufficiently rigorous accuracy tests, so we considered a problem of a non-uniform, rotating flow field in the advective limit. This is sometimes referred to as the “donut problem”. The original variant was proposed in Brooks-Hughes [20]. It is well known that there is no stability issue for this problem. For example, even the Galerkin method performs well for it. However, classical, over-stabilized, full-upwind methods fail miserably. For this problem, the streamline GSC method reduces to SUPG and the results are known to be essentially exact for all cases, so we studied just the directional GSC method and found that the results were also essentially exact for all B-splines and Lagrange elements. Thus, we were encouraged to try to develop a full functional analysis proof of stability, convergence, and error estimates, but we discovered that the method was not coercive in what seemed to be the natural norm. We surmise that the method is *inf-sup* stable but we did not succeed in proving this. In lieu of a proof, we present numerical studies of the *inf-sup* constant and find it to be *inf-sup* stable in a strong norm.

The remainder of the paper is outlined as follows: We introduce the one-dimensional ADR problem in Section 2, describe GSC stabilization in Section 3, and present one-dimensional numerical results and convergence rates in Section 4. Section 5 describes the multidimensional streamline GSC method, numerical evaluations, and the stability and convergence proof and error estimates. We note that the proof has some unique aspects to it which may be of mathematical interest. Section 6 presents the directional GSC method, a suite of test problems, and numerically computed *inf-sup* constants. All the simulation results were obtained using nutils [21], an open source Python programming library. In Section 7, we draw conclusions and identify possible future directions.

2. Galerkin finite element methods for advection-diffusion-reaction problems

The steady advection-diffusion-reaction (ADR) differential operator for advective velocity \mathbf{a} , diffusivity $\kappa > 0$, and reactive rate $r > 0$, reads

$$\mathcal{L}u = ru + \mathbf{a} \cdot \nabla u - \nabla \cdot (\kappa \nabla u), \quad (1)$$

where u is assumed to be a twice-continuously-differentiable function. We frequently refer to two reduced cases, the advection-diffusion (AD) operator, when $r = 0$, and the reaction-diffusion (RD) operator, when $\mathbf{a} = \mathbf{0}$. The differential operator is used to define nonhomogeneous ADR problems on d -dimensional domains $\Omega \subset \mathbb{R}^d$ with boundaries $\Gamma = \partial\Omega$ that are equipped with, for example, Dirichlet data:

$$\begin{aligned} \mathcal{L}u &= f & \text{in } \Omega, \\ u &= g & \text{on } \Gamma. \end{aligned} \quad (2)$$

A homogeneous, one-dimensional ADR problem, with \mathbf{a} , κ , r assumed constant, has an exact solution determined as follows

$$u(\mathbf{x}) \sim \exp(k\mathbf{x}), \quad k \in \mathbb{R}. \quad (3)$$

Values for the parameters k can be computed by substituting the ansatz (3) into Eq. (1) and determining the roots of the resulting characteristic equation

$$r + \mathbf{a}k - \kappa k^2 = 0 \quad (4)$$

$$\implies k_- = \frac{\mathbf{a} + \sqrt{\mathbf{a}^2 + 4r\kappa}}{2\kappa}, \quad k_+ = \frac{\mathbf{a} - \sqrt{\mathbf{a}^2 + 4r\kappa}}{2\kappa}. \tag{5}$$

The exponential functions $\exp(k_- \mathbf{x})$ and $\exp(k_+ \mathbf{x})$ are combined to obtain the exact solution:

$$u(\mathbf{x}) = C_0 \exp(k_- \mathbf{x}) + C_1 \exp(k_+ \mathbf{x}),$$

where the real constants C_0, C_1 are fixed by the boundary conditions. Note that both terms are monotone and, thus, solutions do not oscillate. For example, the solution on the unit interval ($\Omega = [0; 1]$), when equipped with the Dirichlet boundary conditions $u(0) = 0$ and $u(1) = 1$, is given as

$$u(\mathbf{x}) = \exp\left[-\frac{\mathbf{a}(1-\mathbf{x})}{2\kappa}\right] \frac{\sinh(s\mathbf{x})}{\sinh s}, \quad s = \frac{\sqrt{\mathbf{a}^2 + 4r\kappa}}{2\kappa}. \tag{6}$$

Such non-oscillating solutions of ADR problems may be approximated by finite element methods (FEM). The Galerkin FEM approximates the weak formulation of the differential ADR problem in Eq. (2) in terms of

$$\begin{aligned} B^h(u^h, w^h) &= (r w^h, u^h)_{\Omega} + (w^h, \mathbf{a} \cdot \nabla u^h)_{\Omega} + (\kappa \nabla w^h, \nabla u^h)_{\Omega}, \\ L^h(w^h) &= (w^h, f)_{\Omega}, \end{aligned} \tag{7}$$

where u^h and w^h are functions from the approximate solution manifold \mathbb{S}^h and test function space \mathbb{V}^h , respectively, and the notation

$$(f_1, f_2)_D = \int_D f_1 f_2 \, dD$$

is used to denote the integral of two functions f_1, f_2 over the domain D . Based on these forms, the approximate weak formulation of the ADR problems in Eq. (2) reads

$$B^h(u^h, w^h) = L^h(w^h) \quad \text{for all } w^h \in \mathbb{V}^h, \tag{8}$$

where the approximate solution u^h satisfies the Dirichlet conditions. For homogeneous Dirichlet data, $\mathbb{S}^h = \mathbb{V}^h$ and therefore u^h may be expanded in terms of basis functions ω_B and corresponding coefficients \mathbf{d}_B :

$$u^h(\mathbf{x}) = \sum_B \omega_B(\mathbf{x}) \mathbf{d}_B.$$

Using these in Eq. (8) gives

$$\sum_B B^h(\omega_B, \omega_A) \mathbf{d}_B = L^h(\omega_A) \quad \text{for all } \omega_A, \tag{9}$$

which can be solved for the vector of coefficients \mathbf{d} .

Considering the homogeneous one-dimensional case with constant physical parameters, the Galerkin FEM can be analyzed for linear basis functions that are defined on uniform meshes with element size h by considering its computational stencils, i.e., the typical row of the associated systems of linear equations in Eq. (9). In particular, the row that is associated with the basis function ω_A , after multiplication with $\frac{h}{\kappa}$, reads

$$\frac{h}{\kappa} (rS_0 + \mathbf{a}S_1 + \kappa S_2) \begin{bmatrix} \mathbf{d}_{A-1} \\ \mathbf{d}_A \\ \mathbf{d}_{A+1} \end{bmatrix} = 0, \tag{10}$$

where the stencils

$$\begin{aligned} S_0 &= \frac{h}{6} \begin{bmatrix} 1 & 4 & 1 \end{bmatrix}, \\ S_1 &= \frac{1}{2} \begin{bmatrix} -1 & 0 & 1 \end{bmatrix}, \\ S_2 &= \frac{1}{h} \begin{bmatrix} -1 & 2 & -1 \end{bmatrix} \end{aligned} \tag{11}$$

correspond to the discrete zeroth-, first-, and second-order terms in the differential operator \mathcal{L} in Eq. (1). These computational stencils also give rise to a characteristic equation, similar to that of the differential operator in Eq. (4).

In detail, the interpolation property of linear basis functions ω_A at the corresponding nodes $\mathbf{x}_A = hA$

$$\mathbf{d}_A = u^h(hA)$$

and the form of the exact solution u in Eq. (3) suggests that the coefficients follow a power law in the nodal index A :

$$\mathbf{d}_A \sim \theta^A, \quad \theta \in \mathbb{R}. \tag{12}$$

This is substituted into the stencil in Eq. (10) yielding

$$\left(\frac{rh}{\kappa} S_0 + \frac{\mathbf{a}h}{\kappa} S_1 + hS_2 \right) \begin{bmatrix} 1 \\ \theta \\ \theta^2 \end{bmatrix} = \sum_{m=0}^2 \alpha_m \theta^m = 0, \tag{13}$$

where the coefficients

$$\begin{aligned} \alpha_0 &= \frac{Da_h}{6} - \frac{Pe_h}{2} - 1, \\ \alpha_2 &= \alpha_0 + Pe_h = \frac{Da_h}{6} + \frac{Pe_h}{2} - 1, \\ \alpha_1 &= Da_h - (\alpha_0 + \alpha_2) = Da_h - 2\alpha_0 - Pe_h = 2 \left(\frac{Da_h}{3} + 1 \right) \end{aligned}$$

correspond to the first, last, and center terms of the computational stencils in Eq. (11) and the definitions

$$Da_h = \frac{rh^2}{\kappa}, \quad Pe_h = \frac{\mathbf{a}h}{\kappa} \tag{14}$$

are the dimensionless element Damköhler number and element Péclet number, respectively. (Note: There are two common definitions of Damköhler number. The one we utilize is frequently referred to as the *second* Damköhler number.) The two roots of the polynomial in Eq. (13) are

$$\theta_- = \frac{-\alpha_1 + \sqrt{\alpha_1^2 - 4\alpha_2\alpha_0}}{2\alpha_2}, \quad \theta_+ = \frac{-\alpha_1 - \sqrt{\alpha_1^2 - 4\alpha_2\alpha_0}}{2\alpha_2}. \tag{15}$$

If at least one of the roots is negative, i.e., $\theta < 0$, oscillations of the approximate solutions u^h are possible as the power law in Eq. (12) then results in alternating signs of the coefficients \mathbf{d}_A . Such oscillations are indeed encountered in practice when boundary layers are not resolved. For example, considering only the AD operator, the roots in Eq. (15) simplify to

$$\theta_-^{AD} = \frac{2 + |Pe_h|}{2 - Pe_h}, \quad \theta_+^{AD} = \frac{2 - |Pe_h|}{2 - Pe_h}$$

and, therefore, oscillations may be encountered if $|Pe_h| > 2$. Similarly, for the RD operator, Eq. (15) simplifies to

$$\theta_-^{RD} = \frac{2(Da_h + 3)}{6 - Da_h} + \sqrt{\left[\frac{2(Da_h + 3)}{6 - Da_h} \right]^2 - 1}, \quad \theta_+^{RD} = \frac{2(Da_h + 3)}{6 - Da_h} - \sqrt{\left[\frac{2(Da_h + 3)}{6 - Da_h} \right]^2 - 1}$$

and, thus, oscillations potentially occur if $Da_h > 6$. Note that both conditions can be interpreted as constraints on the size of the mesh parameter h . The consequences of not sufficiently resolving boundary layers are exemplified in Fig. 2.1 for the Galerkin FEM applied to pure AD and RD problems.

Sufficiently refined meshes in practical engineering problems are often computationally intractable. Therefore, techniques to eliminate or at least mitigate spurious oscillations are required. The goal is to improve stability and accuracy simultaneously. The approaches developed to this end herein are referred to as GSC stabilization. We consider two types, both of which may be considered generalizations of SUPG stabilization. The first is referred to as **Streamline GSC** and is given by

$$\begin{aligned} B_{GSC}^h(u^h, w^h) &= B^h(u^h, w^h) + (\tau_R \nabla(rw^h), \nabla \mathcal{L}u^h)_{\tilde{\Omega}} + (\tau_A \mathbf{a} \cdot \nabla w^h, \mathcal{L}u^h)_{\tilde{\Omega}}, \\ L_{GSC}^h(w^h) &= L^h(w^h) + (\tau_R \nabla(rw^h), \nabla f)_{\tilde{\Omega}} + (\tau_A \mathbf{a} \cdot \nabla w^h, f)_{\tilde{\Omega}}, \end{aligned}$$

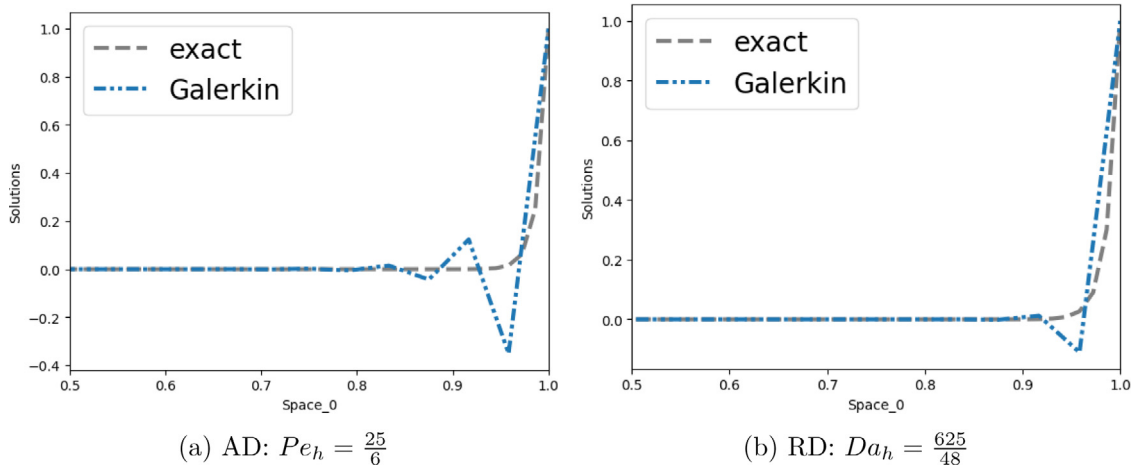


Fig. 2.1. Oscillating linear finite element solutions computed with the Galerkin method.

where τ_R and τ_A are the reactive and advective stabilization parameters and

$$\tilde{\Omega} = \bigcup_e \Omega^e$$

denotes the union of all element interiors Ω^e , i.e., the boundaries of the elements e are excluded. Note that the advective stabilization term is of SUPG type and the reactive stabilization term acts on the gradient of the residual. The streamline GSC method leads to the following system of linear equations

$$\sum_B B_{GSC}^h(\omega_B, \omega_A) \mathbf{d}_B = L_{GSC}^h(\omega_A) \quad \text{for all } \omega_A. \tag{16}$$

The next section considers choices of stabilization parameters τ_R, τ_A that yield non-oscillating approximate solutions.

The second type of GSC method, directional GSC, will be described subsequently. In one dimension, the streamline GSC and directional GSC methods are identical, and therefore in the following sections concerning the one-dimensional problem, we just refer to the method as GSC.

3. Stabilization for one-dimensional advection-diffusion-reaction problems

The stabilization parameters τ_R, τ_A can be chosen for bases having the interpolation property such that the solutions are nodally exact, that is, $\mathbf{d}_A = u^h(\mathbf{x}_A) = u(hA)$. Stabilization parameters can be determined for homogeneous one-dimensional ADR problems with constant physical parameters in three steps. The approach presented here is new in that it applies to higher-order nodal finite elements as well as linear elements. However, we will develop it just for linear elements for simplicity and because that is all we will use in the remainder of this paper. First, an analogue to Eq. (10), that is, the typical row of the linear equation system, is derived for the GSC method. Second, the roots θ in the power law in Eq. (12) are replaced by exponential functions of the two characteristic roots, $\exp(k_-h)$ and $\exp(k_+h)$. Third, the coefficients are accordingly replaced in the row that is associated with the basis function ω_A resulting in two equations

$$\begin{aligned} \left[\frac{rh}{\kappa} S_0 + \frac{ah}{\kappa} (1 - \tau_A r) S_1 + h \left(1 + \frac{\tau_R r^2}{\kappa} + \frac{\tau_A a^2}{\kappa} \right) S_2 \right] \begin{bmatrix} 1 \\ \exp(k_-h) \\ \exp(2k_-h) \end{bmatrix} &= 0, \\ \left[\frac{rh}{\kappa} S_0 + \frac{ah}{\kappa} (1 - \tau_A r) S_1 + h \left(1 + \frac{\tau_R r^2}{\kappa} + \frac{\tau_A a^2}{\kappa} \right) S_2 \right] \begin{bmatrix} 1 \\ \exp(k_+h) \\ \exp(2k_+h) \end{bmatrix} &= 0. \end{aligned} \tag{17}$$

Note that these two equations, as well as the characteristic roots in Eq. (5), can be written in terms of the dimensionless numbers in Eq. (14) as

$$\sum_{m=0}^2 \alpha_m \exp \left\{ m \left[\frac{Pe_h}{2} + \sqrt{\left(\frac{Pe_h}{2}\right)^2 + Da_h} \right] \right\} = 0, \tag{18}$$

$$\sum_{m=0}^2 \alpha_m \exp \left\{ m \left[\frac{Pe_h}{2} - \sqrt{\left(\frac{Pe_h}{2}\right)^2 + Da_h} \right] \right\} = 0,$$

with the coefficients

$$\alpha_0 = \frac{Da_h}{6} - \frac{Pe_h}{2} (1 - \tau_{Ar}) - \left(1 + \frac{\tau_{Rr}^2}{\kappa} + \frac{\tau_A \mathbf{a}^2}{\kappa} \right),$$

$$\alpha_2 = \alpha_0 + Pe_h (1 - \tau_{Ar}) = \frac{Da_h}{6} + \frac{Pe_h}{2} (1 - \tau_{Ar}) - \left(1 + \frac{\tau_{Rr}^2}{\kappa} + \frac{\tau_A \mathbf{a}^2}{\kappa} \right),$$

$$\alpha_1 = Da_h - (\alpha_0 + \alpha_2) = Da_h - 2\alpha_0 - Pe_h (1 - \tau_{Ar}) = 2 \left(\frac{Da_h}{3} + 1 + \frac{\tau_{Rr}^2}{\kappa} + \frac{\tau_A \mathbf{a}^2}{\kappa} \right).$$

This pair of reformulated equations is considered in the following sections to solve for the stabilization parameters τ_R, τ_A in terms of their nondimensional counterparts

$$\chi = \frac{r}{h^2} \tau_R, \tag{19}$$

$$\zeta = \frac{\mathbf{a}}{h} \tau_A.$$

3.1. Advection-diffusion

First, consider the AD problem. Eq. (18) simplifies to

$$\sum_{m=0}^2 \alpha_m \exp \left\{ m \left[\frac{Pe_h}{2} + \frac{Pe_h}{2} \right] \right\} = 0, \quad \sum_{m=0}^2 \alpha_m \exp \left\{ m \left[\frac{Pe_h}{2} - \frac{Pe_h}{2} \right] \right\} = 0,$$

with the coefficients

$$\alpha_0 = -\frac{Pe_h}{2} - \left(1 + \frac{\tau_A \mathbf{a}^2}{\kappa} \right),$$

$$\alpha_2 = \alpha_0 + Pe_h = \frac{Pe_h}{2} - \left(1 + \frac{\tau_A \mathbf{a}^2}{\kappa} \right),$$

$$\alpha_1 = -(\alpha_0 + \alpha_2) = -2\alpha_0 - Pe_h = 2 \left(1 + \frac{\tau_A \mathbf{a}^2}{\kappa} \right).$$

Note that the second equation is always satisfied and the first equation yields the classical nondimensional advective stabilization parameter for the AD problem

$$\zeta^{AD} = \frac{\coth(0.5 Pe_h)}{2} - \frac{1}{Pe_h} \tag{20}$$

shown in Fig. 3.1.

3.2. Reaction-diffusion

Consider the RD problem. Eq. (18) simplifies to

$$\sum_{m=0}^2 \alpha_m \exp \left\{ m \sqrt{Da_h} \right\} = 0, \quad \sum_{m=0}^2 \alpha_m \exp \left\{ -m \sqrt{Da_h} \right\} = 0,$$

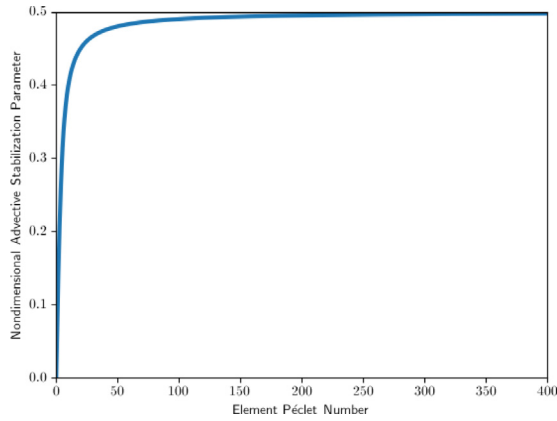


Fig. 3.1. Exact nondimensional advective stabilization parameter ζ^{AD} for the GSC method for the AD problem in one dimension.

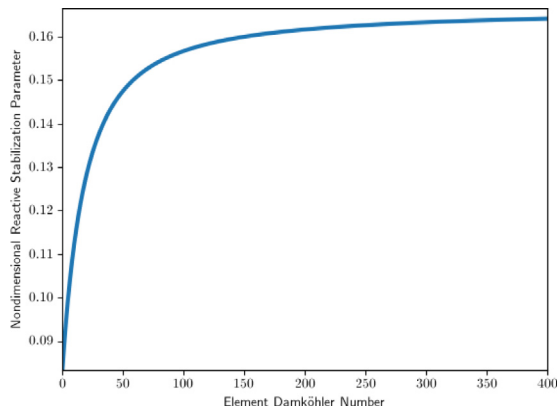


Fig. 3.2. Exact nondimensional reactive stabilization parameter χ^{RD} for the GSC method for the RD problem in one dimension.

with the coefficients

$$\alpha_0 = \frac{Da_h}{6} - \left(1 + \frac{\tau_R r^2}{\kappa}\right),$$

$$\alpha_2 = \alpha_0 = \frac{Da_h}{6} - \left(1 + \frac{\tau_R r^2}{\kappa}\right),$$

$$\alpha_1 = Da_h - (\alpha_0 + \alpha_2) = Da_h - 2\alpha_0 = 2 \left(\frac{Da_h}{3} + 1 + \frac{\tau_R r^2}{\kappa} \right).$$

Since $\alpha_2 = \alpha_0$, multiplying both sides of the first equation by $\exp(-2\sqrt{Da_h})$ yields the second equation and we only need to solve one of them to obtain the nondimensional reactive stabilization parameter for the RD problem

$$\chi^{RD} = \frac{1}{6} + \frac{1}{2(\cosh \sqrt{Da_h} - 1)} - \frac{1}{Da_h} \tag{21}$$

shown in Fig. 3.2.

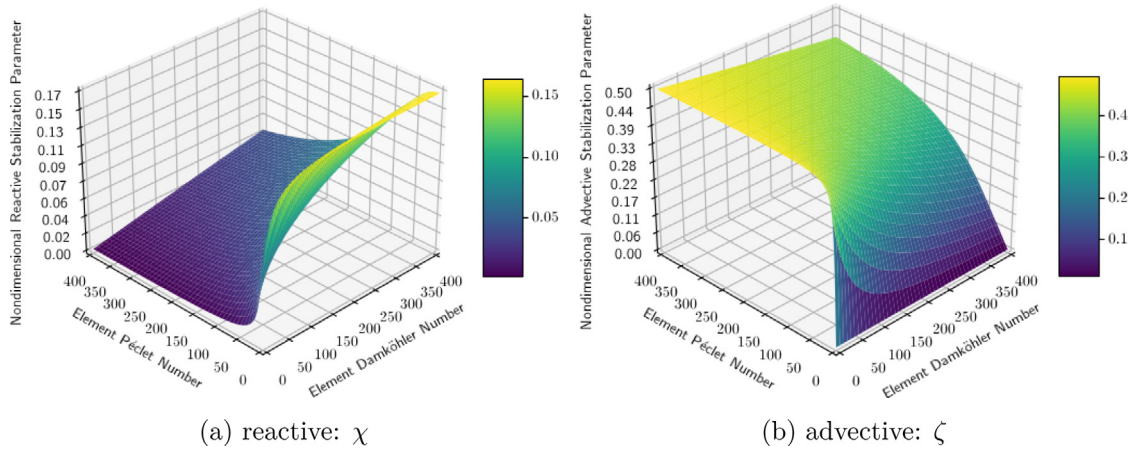


Fig. 3.3. Exact nondimensional stabilization parameters for the GSC method for the ADR problem in one dimension.

3.3. Advection-diffusion-reaction

Consider the ADR problem. This time both equations in Eq. (18) must be solved. Their solutions are the nondimensional stabilization parameters for the ADR problem

$$\chi = \frac{1}{6} + \frac{\cosh(0.5Pe_h)}{2 \left[\cosh \sqrt{0.25Pe_h^2 + Da_h} - \cosh(0.5Pe_h) \right]} - \frac{1 + Pe_h \zeta}{Da_h}, \tag{22}$$

$$\zeta = \frac{Pe_h}{Da_h} - \frac{\sinh(0.5Pe_h)}{\cosh \sqrt{0.25Pe_h^2 + Da_h} - \cosh(0.5Pe_h)}$$

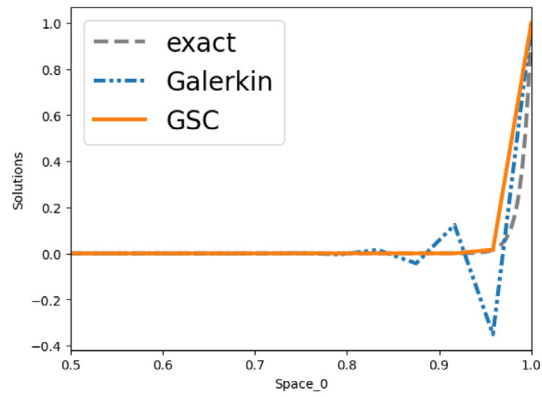
and are shown in Fig. 3.3.

4. Results for one-dimensional advection-diffusion-reaction problems

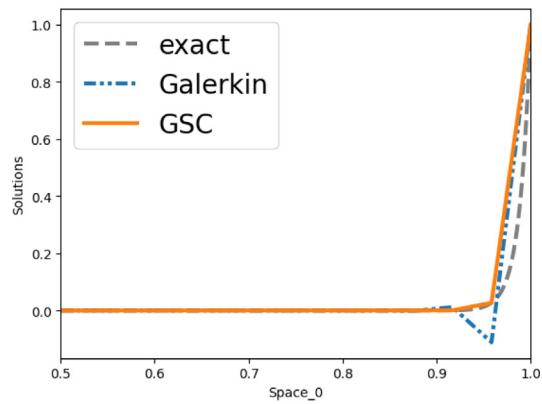
GSC and Galerkin solutions of the AD and RD problems introduced in Section 2 as well as the corresponding ADR problem are shown in Fig. 4.1 for linear finite elements. Solutions for quadratic, cubic, and quartic Lagrange elements, as well as maximally-smooth B-spline basis functions, are presented in Figs. 4.2, 4.3, and 4.4, respectively. (Note that for the higher-order basis functions we have again used the same stabilization parameters in the GSC method that were derived for linear finite elements, which is motivated by the results of [19].) Each simulation has 25 degrees of freedom, meaning that the element sizes h increase with the order of the bases (but to a lesser extent for B-splines than Lagrange elements). Galerkin FEM results show oscillations, as expected because the element Damköhler and Péclet numbers Da_h and Pe_h are greater than thirteen and four, respectively. For higher-order basis functions, the figures show that B-spline solutions resolve the boundary layers better than Lagrange solutions. In all cases, the GSC method gives a monotone solution.

Convergence results for the L^2 norm and H^1 semi-norm for the AD, RD, and ADR problems are shown in Fig. 4.5. The corresponding convergence rates are listed in Table 4.1. The numbers of degrees of freedom were $1 + 4!2^n$ where $n = 0, \dots, 8$, i.e., 25 ($n = 0$) and 6145 ($n = 8$) for the coarsest and finest simulations, respectively. For the most part, the B-spline results are more accurate than the Lagrange results for the same polynomial order, p . The H^1 convergence rates presented in Table 4.1 are optimal, that is, $\mathcal{O}(h^p)$, but not all are $\mathcal{O}(h^{p+1})$ in L^2 . The L^2 rate of convergence is not determined by the derivation of the stabilization parameters, except for the linear element case, which is optimal because it is the nodal interpolate.

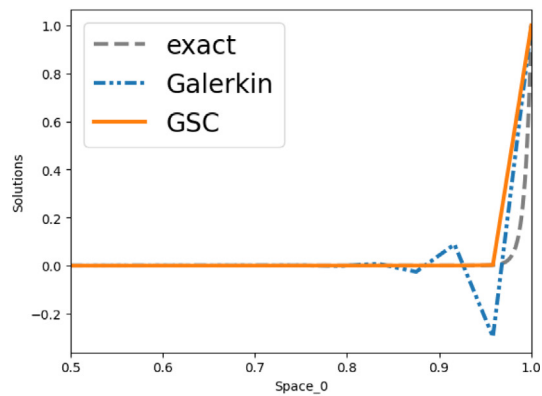
Given the sensitivity of the exact GSC stabilization parameters, as noted previously, we endeavored to create numerically stable approximations to the exact ones. As will be seen, the approximate stabilization parameters



(a) AD

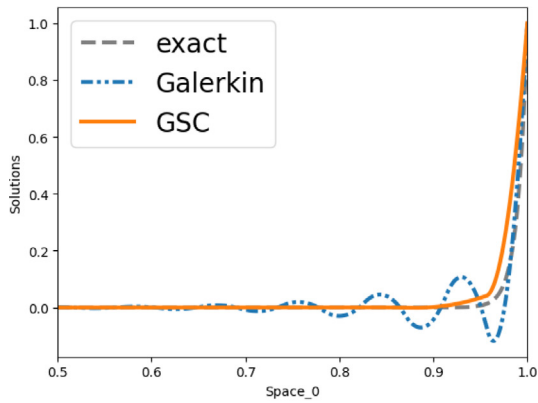


(b) RD

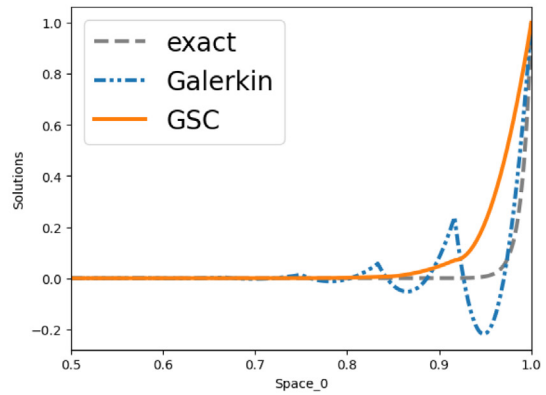


(c) ADR

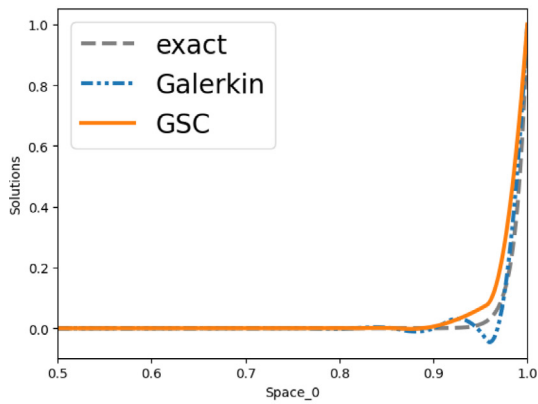
Fig. 4.1. Linear finite element solutions computed with Galerkin and GSC methods for reactive rate $r = 7.5 \times 10^3 \text{ s}^{-1}$, advective velocity $\mathbf{a} = 1.0 \times 10^2 \text{ m s}^{-1}$, and diffusivity $\kappa = 1.0 \text{ m}^2 \text{ s}^{-1}$. The stabilization parameters for one-dimensional AD, RD, and ADR problems are given in Eqs. (20), (21), and (22), respectively.



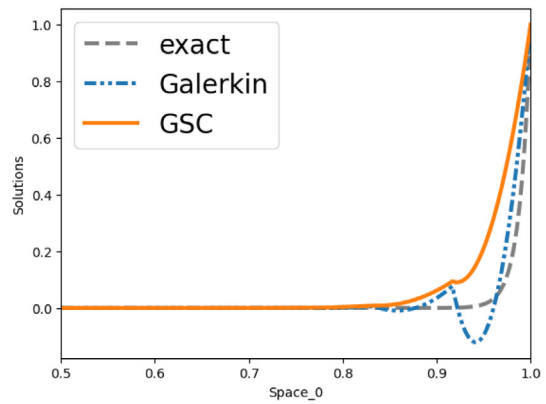
(a) AD: B-spline



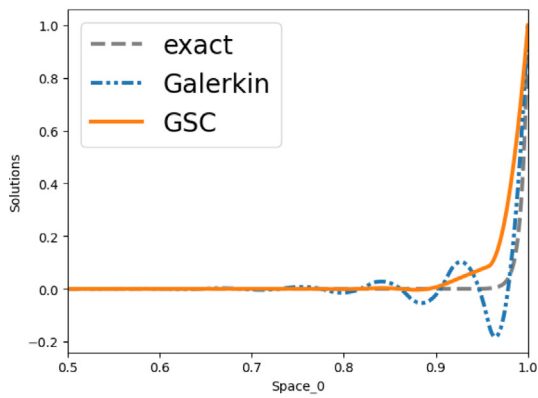
(b) AD: Lagrange



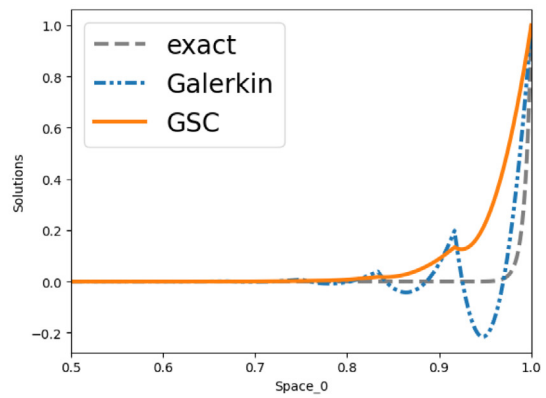
(c) RD: B-spline



(d) RD: Lagrange

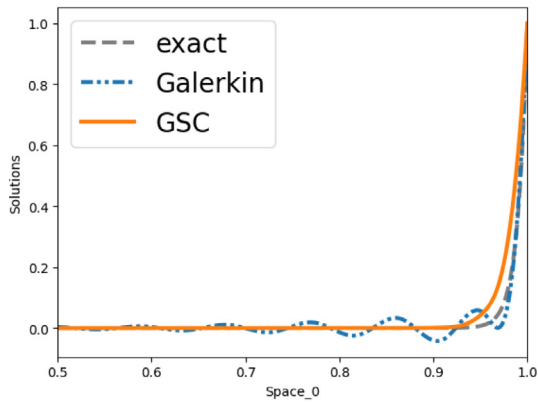


(e) ADR: B-spline

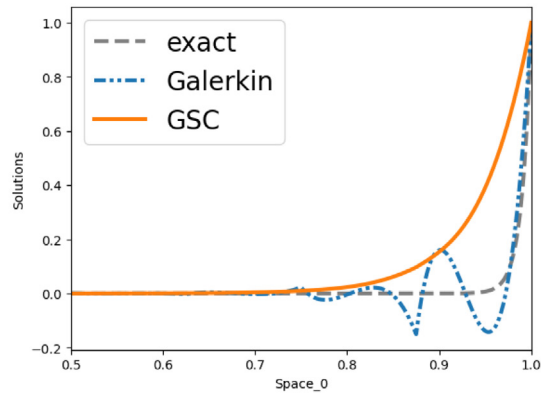


(f) ADR: Lagrange

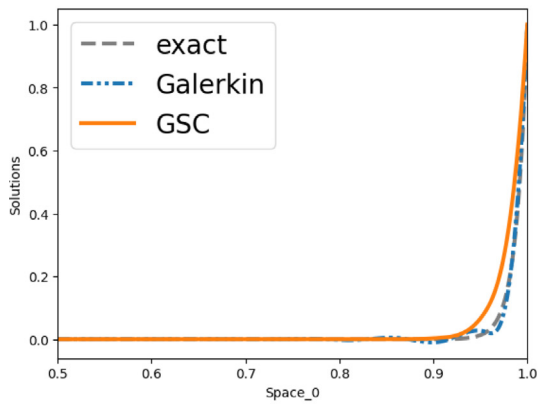
Fig. 4.2. Quadratic approximate solutions computed with Galerkin and GSC methods for reactive rate $r = 7.5 \times 10^3 \text{ s}^{-1}$, advective velocity $\mathbf{a} = 1.0 \times 10^2 \text{ m s}^{-1}$, and diffusivity $\kappa = 1.0 \text{ m}^2 \text{ s}^{-1}$. The stabilization parameters for one-dimensional AD, RD, and ADR problems are given in Eqs. (20), (21), and (22), respectively.



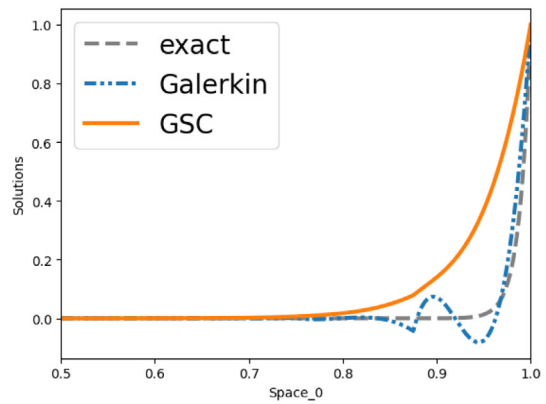
(a) AD: B-spline



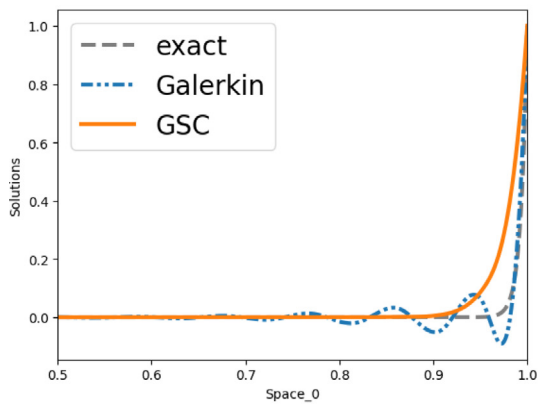
(b) AD: Lagrange



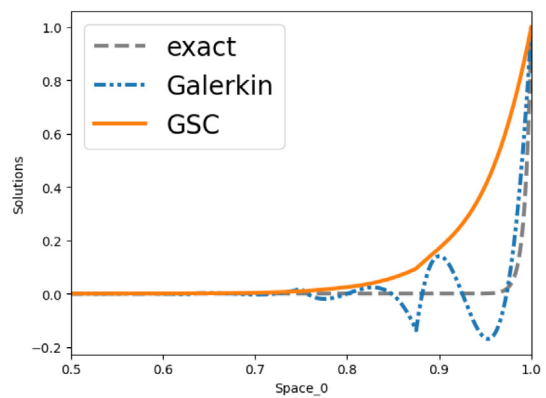
(c) RD: B-spline



(d) RD: Lagrange

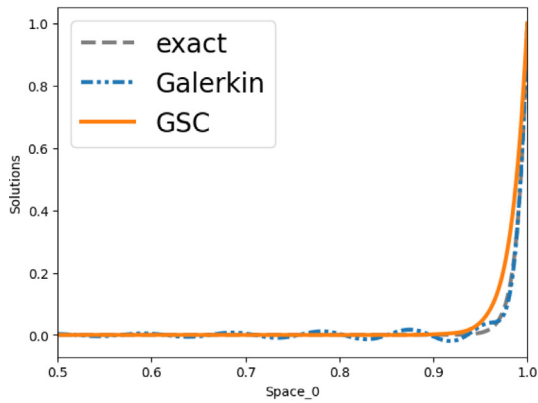


(e) ADR: B-spline

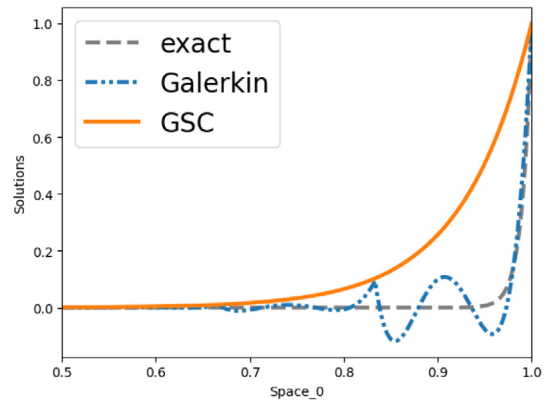


(f) ADR: Lagrange

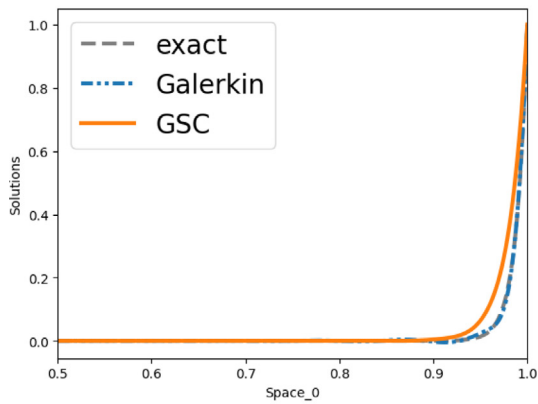
Fig. 4.3. Cubic approximate solutions computed with Galerkin and GSC methods for reactive rate $r = 7.5 \times 10^3 \text{ s}^{-1}$, advective velocity $\mathbf{a} = 1.0 \times 10^2 \text{ m s}^{-1}$, and diffusivity $\kappa = 1.0 \text{ m}^2 \text{ s}^{-1}$. The stabilization parameters for one-dimensional AD, RD, and ADR problems are given in Eqs. (20), (21), and (22), respectively.



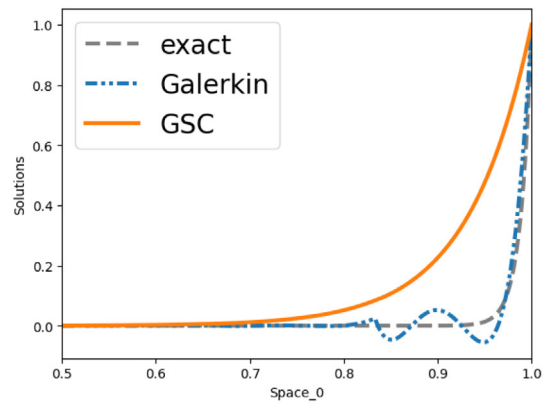
(a) AD: B-spline



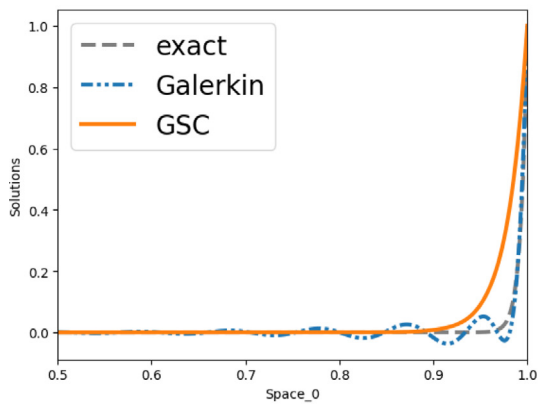
(b) AD: Lagrange



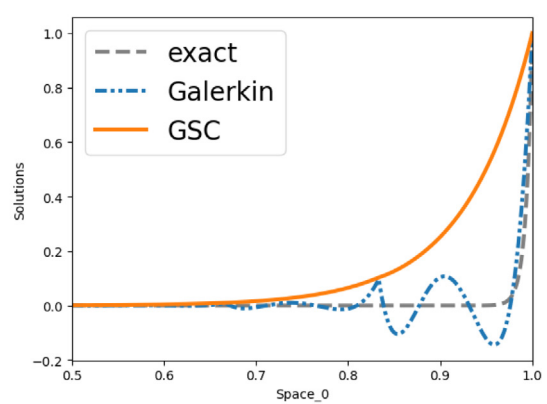
(c) RD: B-spline



(d) RD: Lagrange

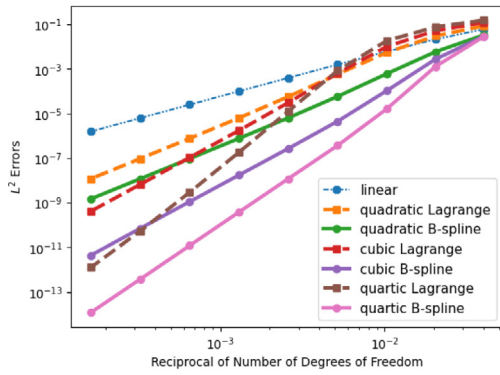


(e) ADR: B-spline

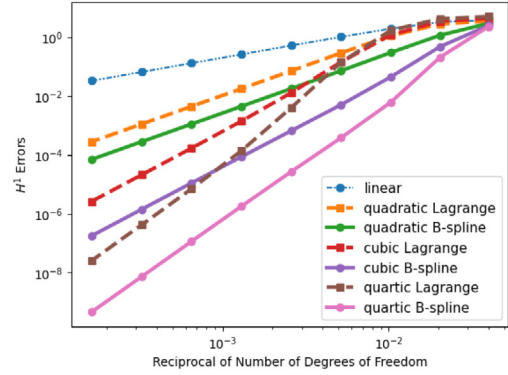


(f) ADR: Lagrange

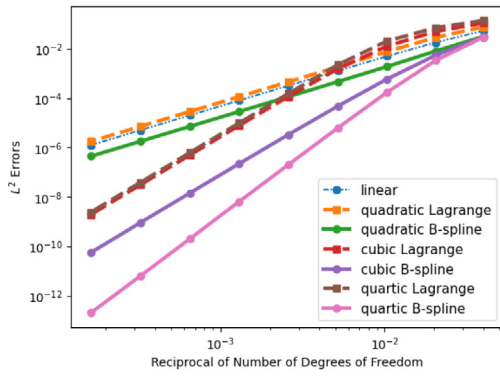
Fig. 4.4. Quartic approximate solutions computed with Galerkin and GSC methods for reactive rate $r = 7.5 \times 10^3 \text{ s}^{-1}$, advective velocity $\mathbf{a} = 1.0 \times 10^2 \text{ m s}^{-1}$, and diffusivity $\kappa = 1.0 \text{ m}^2 \text{ s}^{-1}$. The stabilization parameters for one-dimensional AD, RD, and ADR problems are given in Eqs. (20), (21), and (22), respectively.



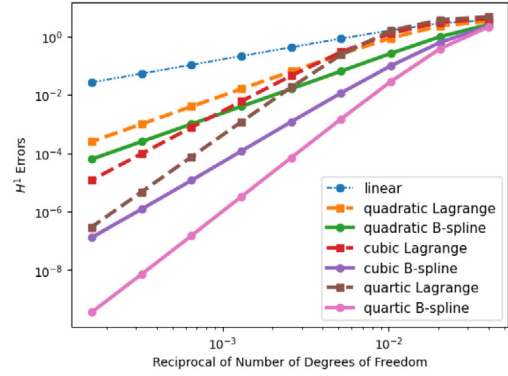
(a) AD: L^2



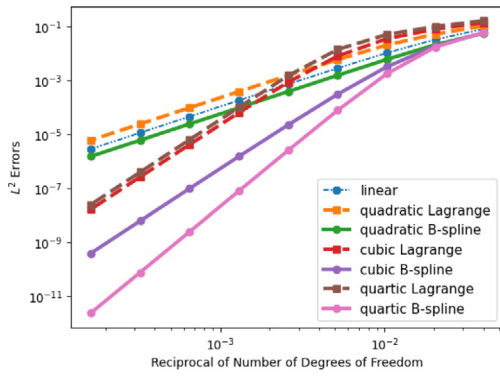
(b) AD: H^1



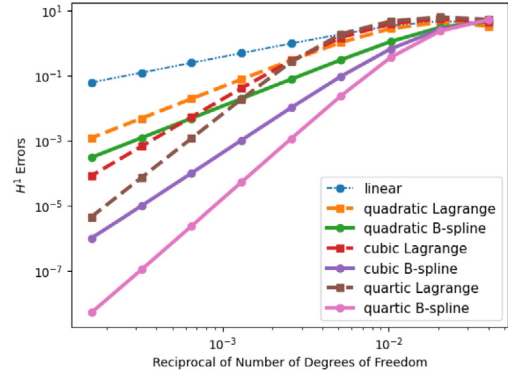
(c) RD: L^2



(d) RD: H^1



(e) ADR: L^2



(f) ADR: H^1

Fig. 4.5. Convergence analyses (25, 49, 97, 193, 385, 769, 1537, 3073, and 6145 degrees of freedom) in the L^2 norm and H^1 semi-norm for the one-dimensional GSC method for reactive rate $r = 7.5 \times 10^3 \text{ s}^{-1}$, advective velocity $\mathbf{a} = 1.0 \times 10^2 \text{ m s}^{-1}$, and diffusivity $\kappa = 1.0 \text{ m}^2 \text{ s}^{-1}$. The stabilization parameters for one-dimensional AD, RD, and ADR problems are given in Eqs. (20), (21), and (22), respectively. Corresponding convergence rates are listed in Table 4.1.

Table 4.1

Convergence rates for the one-dimensional GSC method in the L^2 norm and H^1 semi-norm based on the two most refined simulations (3073 and 6145 degrees of freedom) for each case and basis (see Fig. 4.5). The stabilization parameters for one-dimensional AD, RD, and ADR problems are given in Eqs. (20), (21), and (22), respectively.

Order	Basis	AD		RD		ADR	
		L^2	H^1	L^2	H^1	L^2	H^1
Linear	B-spline/ Lagrange	2.000	1.000	2.000	1.000	2.000	1.000
Quadratic	B-spline	3.002	2.001	2.001	2.001	2.001	2.001
	Lagrange	3.005	2.001	2.001	2.000	2.000	2.000
Cubic	B-spline	3.993	2.993	3.990	3.210	3.991	3.275
	Lagrange	4.003	3.005	4.000	3.000	3.997	2.998
Quartic	B-spline	4.974	3.994	4.946	4.327	5.006	4.388
	Lagrange	5.409	4.021	4.000	4.000	4.001	4.003

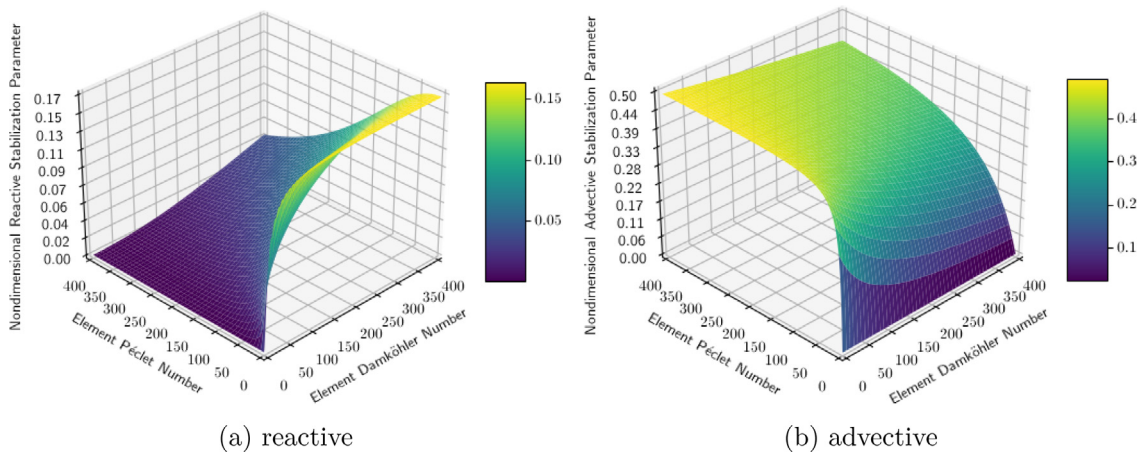


Fig. 4.6. Approximations to the exact nondimensional stabilization parameters in GSC methods depicted in Fig. 3.3.

achieve optimal convergence rates in L^2 and H^1 for all cases considered. The approximate parameters are given by the following formulas:

$$\chi \approx \frac{Da_h^2}{6Da_h^2 + 36Da_h + 216 + 19.2323Pe_h^2}, \tag{23}$$

$$\zeta \approx \frac{Pe_h}{2|Pe_h| + 12 + 0.392211Da_h}.$$

The parameters in Eq. (23) approximate the nondimensional stabilization parameters in Eq. (22) quite well as can be verified by considering their plots in Fig. 4.6 and by comparing their corresponding slices in Fig. 4.7 for several element Damköhler numbers Da_h . Their precise forms are rationalized by considering Taylor and Laurent expansions, as follows:

The reactive limit $Pe_h \rightarrow 0$ of the nondimensional reactive stabilization parameter χ in Eq. (22) is the RD result χ^{RD} in Eq. (21) that can be well-approximated by the harmonic-mean-like expression

$$\chi^{RD} \approx \frac{Da_h^2}{6Da_h^2 + 36Da_h + 216}, \tag{24}$$

which has the correct asymptotic value and first two derivatives for $Da_h \rightarrow \infty$. For the advective limit $Da_h \rightarrow 0$, this approximation asymptotes to zero instead of $\frac{\zeta^{AD}}{Pe_h}$ (the limit of the corresponding exact reactive stabilization

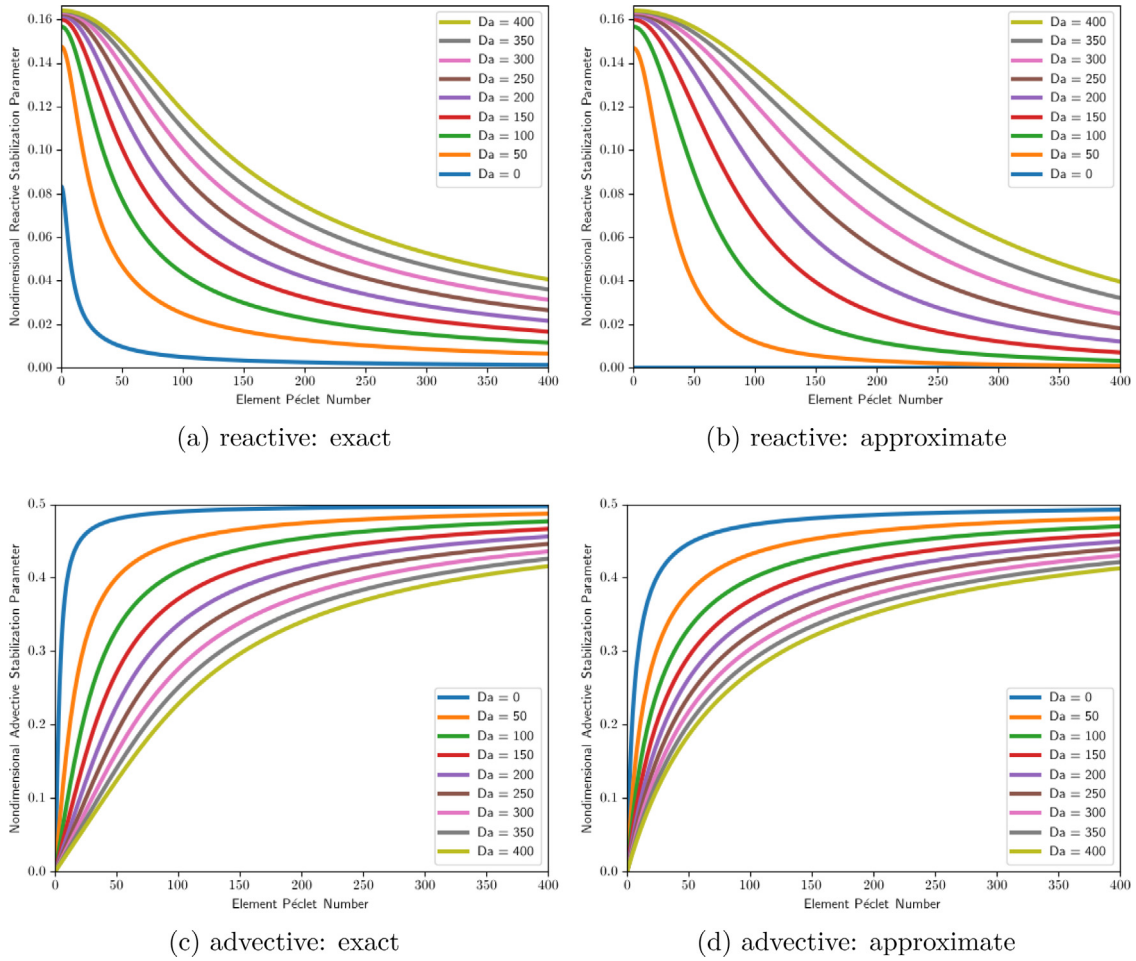


Fig. 4.7. For element Damköhler numbers $Da_h \in \{0, 50, \dots, 400\}$: slices of the exact and approximate nondimensional stabilization parameters in GSC methods.

parameter χ , see Appendix A). The additional Pe_h^2 -contribution in Eq. (23) facilitates approximately obtaining the asymptotic value $(\frac{14-5e}{6(e-1)})$, where e is Euler’s number) for the reactive-advective limit $Da_h \rightarrow \infty, Pe_h \rightarrow \infty$.

The advective limit $Da_h \rightarrow 0$ of the nondimensional advective stabilization parameter ζ in Eq. (22) is the AD result ζ^{AD} in Eq. (20) that can be approximated by the following harmonic-mean-like formula:

$$\zeta^{AD} \approx \frac{Pe_h}{2|Pe_h| + 12}. \tag{25}$$

This ensures a zero value at $Pe_h = 0$, the correct limit $(\frac{1}{2})$ for $Pe_h \rightarrow \infty$, the correct slope $(\frac{1}{12})$ at $Pe_h = 0$, and smoothness of the approximation. Also, this approximation of ζ^{AD} already conforms to the reactive limit $Pe_h \rightarrow 0$ of the exact advective stabilization parameter ζ , because it vanishes for $Pe_h = 0$. The additional Da_h -contribution in Eq. (23) allows to approximately obtain an adequate asymptotic value $(\frac{e-2}{e-1})$, where e is Euler’s number) for the reactive-advective limit $Da_h \rightarrow \infty, Pe_h \rightarrow \infty$.

We repeated the above numerical evaluation for the approximate stabilization parameters. GSC and Galerkin solutions of the AD, RD, and ADR problems are shown in Fig. 4.8 for linear finite elements. Note, the results are no longer monotone for this case. Solutions for quadratic, cubic, and quartic Lagrange and maximally smooth B-spline elements are presented in Figs. 4.9, 4.10, and 4.11, respectively. Using the approximate stabilization for linear finite elements once again for higher-order elements, the solutions become more monotone as the order increases. The corresponding convergence results and rates for the L^2 norm and H^1 semi-norm are shown in Fig. 4.12 and

Table 4.2

Convergence rates for the one-dimensional GSC method in the L^2 norm and H^1 semi-norm based on the two most refined simulations (3073 and 6145 degrees of freedom) for each case and basis (see Fig. 4.12). The stabilization parameters for one-dimensional ADR, RD, and AD problems are approximated according to Eqs. (23), (24), and (25), respectively.

Order	Basis	AD		RD		ADR	
		L^2	H^1	L^2	H^1	L^2	H^1
Linear	B-spline/ Lagrange	1.998	1.000	2.000	1.000	1.999	1.000
Quadratic	B-spline	3.002	2.001	3.002	2.001	3.003	2.001
	Lagrange	3.004	2.001	3.000	2.000	3.003	2.000
Cubic	B-spline	3.993	2.993	3.994	2.994	3.988	2.989
	Lagrange	3.993	3.005	4.000	3.000	3.994	3.003
Quartic	B-spline	4.973	3.994	4.571	3.995	4.990	3.988
	Lagrange	5.426	4.020	5.000	4.000	5.226	4.018

listed in Table 4.2. For the approximate stabilization parameters, all the convergence rates are optimal, although for quartic B-splines in the RD case it is ostensibly suboptimal, that is, 4.571. However, examination of the convergence results revealed that the optimal convergence rate of 5 was obtained for several meshes prior to the most refined one, where the accuracy was approximately 14 digits and likely affected by round-off errors.

This section tested two sets of formulas that were derived for linear finite elements corresponding to exact and approximate stabilization parameters. The exact formulas guarantee nodal exactness for linear basis functions in one-dimensional problems, but they did not yield optimal convergence rates for higher-order basis functions for reactive problems and involve exponential functions that are computationally challenging. The approximate formulas did not yield nodal exactness for linear basis functions in one-dimensional problems, but they resulted in optimal convergence rates for all basis functions and are robust and computationally efficient. In conclusion, we advocate the use of the exact formulas for linear finite elements but the approximate formulas in all other cases. They are used in the multidimensional problems throughout the remainder of this paper.

5. Streamline GSC method

To obtain numerical results with the streamline GSC method for multidimensional problems, the one-dimensional stabilization parameters τ_R , τ_A must be generalized to multiple dimensions. Consistent with the generalization of the element Péclet number

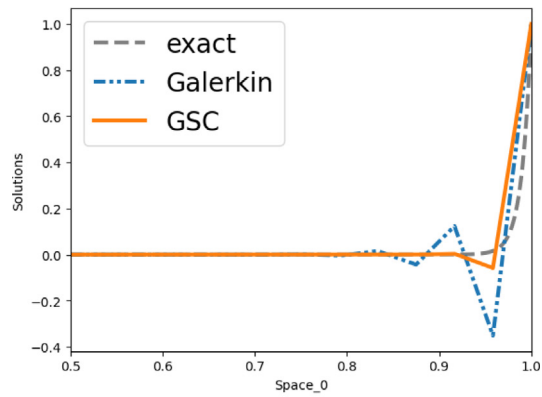
$$Pe_h = \frac{\|\mathbf{a}\|_2 h}{\kappa},$$

the advective velocity \mathbf{a} is represented by its Euclidean norm $\|\mathbf{a}\|_2$, i.e.,

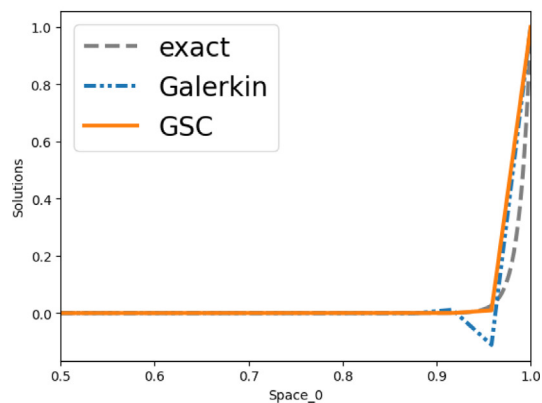
$$\tau_A = \frac{h}{\|\mathbf{a}\|_2} \zeta.$$

The streamline GSC method is schematically illustrated in Table 5.1. The black arrow in the diagram represents the velocity \mathbf{a} and indicates that the stabilization is performed in the streamline direction.

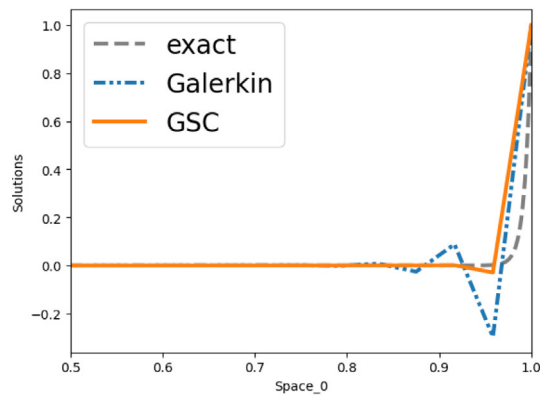
We consider the classic Advection-Skew-to-Mesh problem depicted in Fig. 5.1. In particular, we consider the unit square and a flow angle $\theta = 30^\circ$. Numerical results for the streamline GSC method, using the approximate stabilization parameters described previously, are presented in Fig. 5.2 along with results for the Galerkin method for which the faint icon indicates that no stabilization is added. Exactly the same stabilization parameters are employed for all quadratic, cubic, and quartic Lagrange and B-spline elements shown in Figs. 5.3, 5.4, and 5.5, respectively. We utilize 625 degrees of freedom in each simulation, meaning that the element sizes h increase with the order of the bases. Galerkin FEM results show oscillations as expected because the element Damköhler and Péclet numbers are greater than thirteen and forty, respectively. For higher-order basis functions, B-spline solutions resolve the boundary layers better than Lagrange solutions, which are overly diffuse. In all cases the streamline GSC method performs well. Minimum and maximum values of the solutions for the AD, RD, and ADR problems are listed



(a) AD



(b) RD

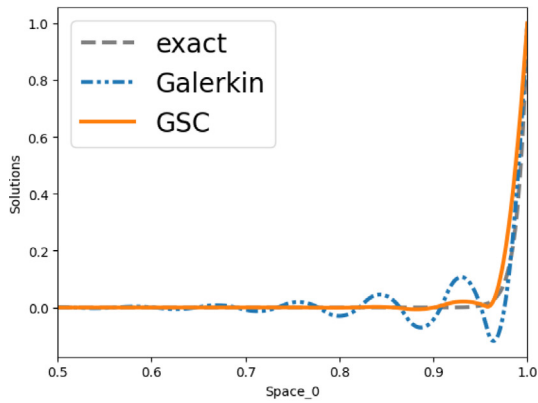


(c) ADR

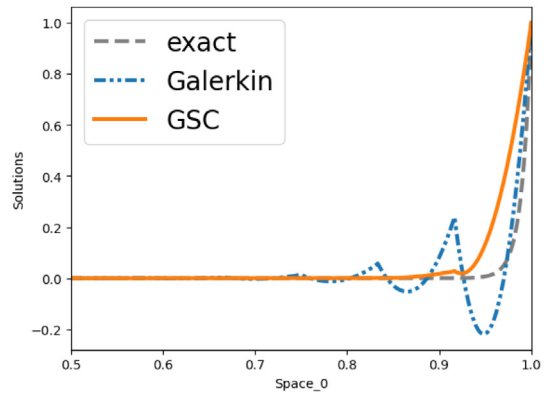
Fig. 4.8. Linear finite element solutions computed with Galerkin and GSC methods for reactive rate $r = 7.5 \times 10^3 \text{ s}^{-1}$, advective velocity $\mathbf{a} = 1.0 \times 10^2 \text{ m s}^{-1}$, and diffusivity $\kappa = 1.0 \text{ m}^2 \text{ s}^{-1}$. The stabilization parameters for one-dimensional ADR, RD, and AD problems are approximated according to Eqs. (23), (24), and (25), respectively.

in Table 5.2. Note that the minima and maxima for B-spline elements are always smaller in magnitude than for Lagrange elements.

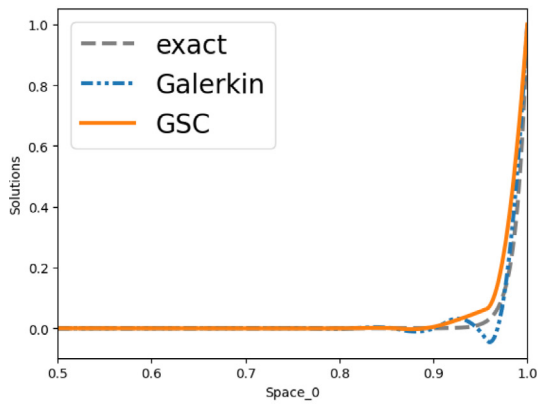
We will now provide a proof of stability and convergence for the streamline GSC method in the multidimensional setting for arbitrary-order finite elements.



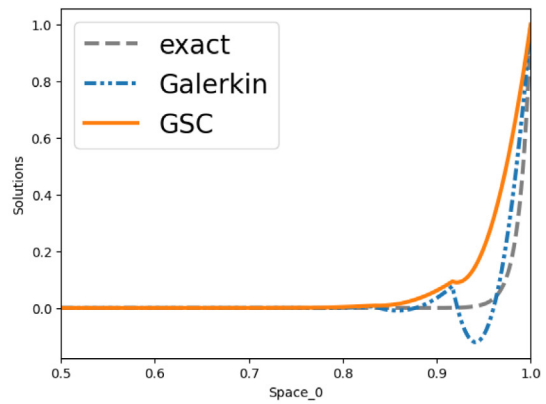
(a) AD: B-spline



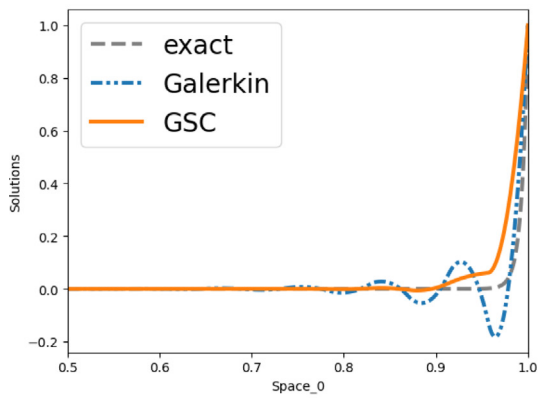
(b) AD: Lagrange



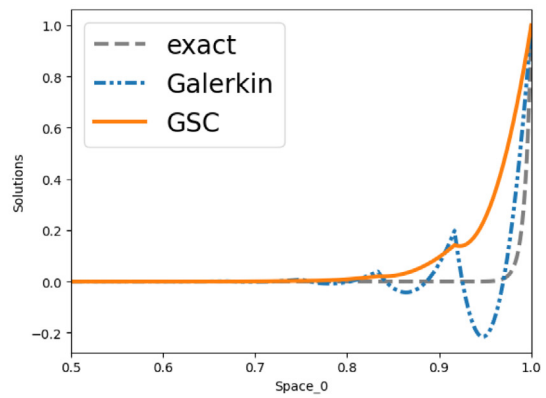
(c) RD: B-spline



(d) RD: Lagrange

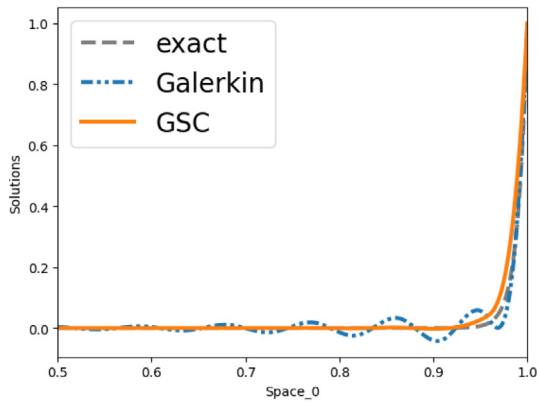


(e) ADR: B-spline

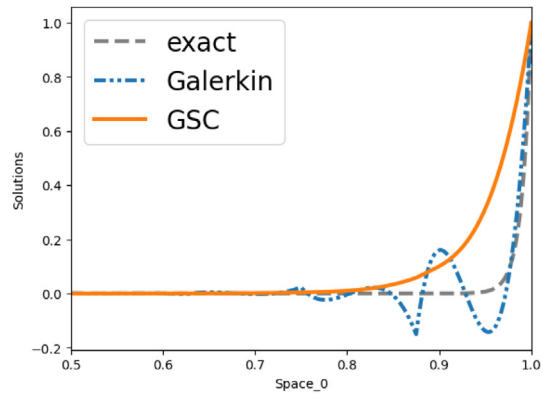


(f) ADR: Lagrange

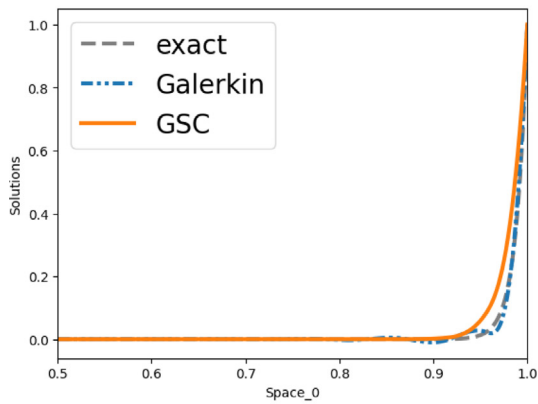
Fig. 4.9. Quadratic approximate solutions computed with Galerkin and GSC methods for reactive rate $r = 7.5 \times 10^3 \text{ s}^{-1}$, advective velocity $\mathbf{a} = 1.0 \times 10^2 \text{ m s}^{-1}$, and diffusivity $\kappa = 1.0 \text{ m}^2 \text{ s}^{-1}$. The stabilization parameters for one-dimensional ADR, RD, and AD problems are approximated according to Eqs. (23), (24), and (25), respectively.



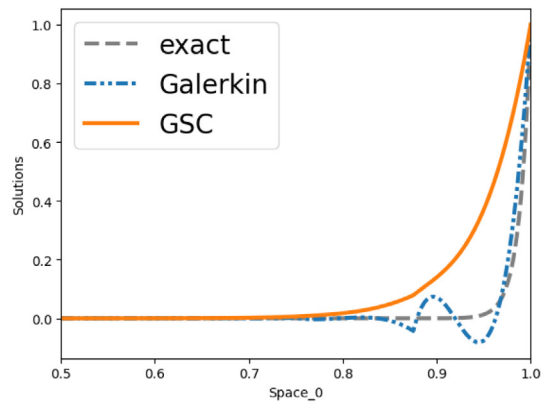
(a) AD: B-spline



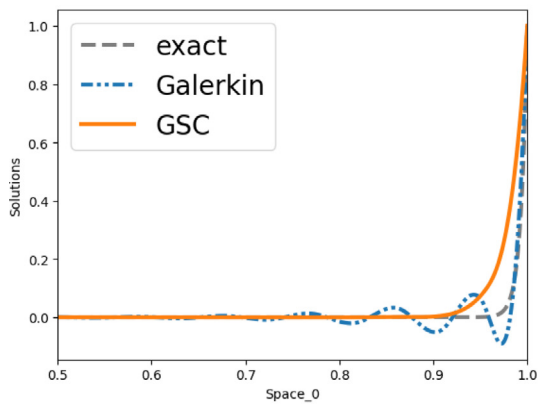
(b) AD: Lagrange



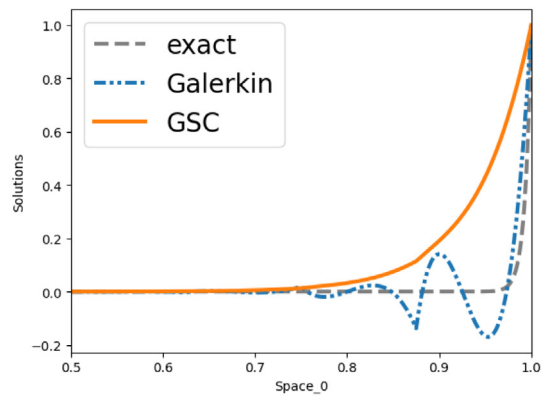
(c) RD: B-spline



(d) RD: Lagrange

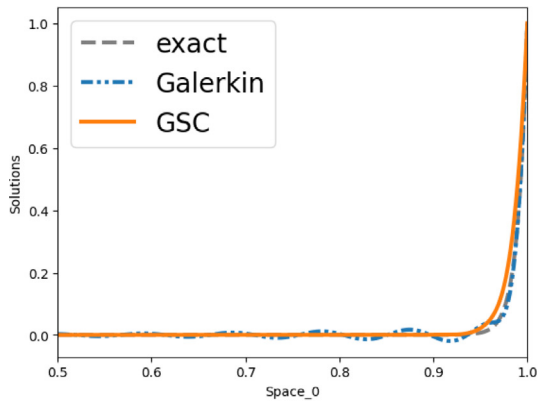


(e) ADR: B-spline

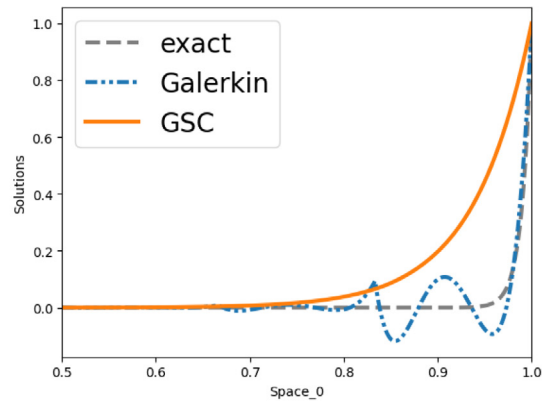


(f) ADR: Lagrange

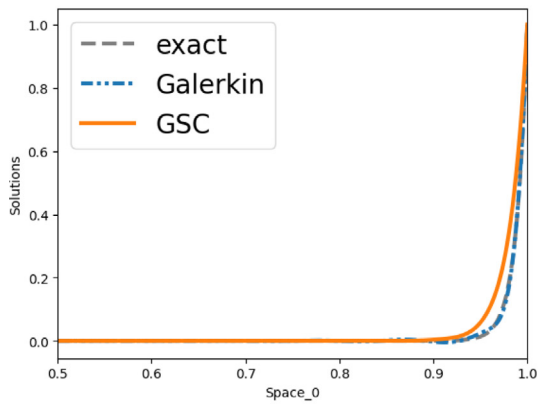
Fig. 4.10. Cubic approximate solutions computed with Galerkin and GSC methods for reactive rate $r = 7.5 \times 10^3 \text{ s}^{-1}$, advective velocity $\mathbf{a} = 1.0 \times 10^2 \text{ m s}^{-1}$, and diffusivity $\kappa = 1.0 \text{ m}^2 \text{ s}^{-1}$. The stabilization parameters for one-dimensional ADR, RD, and AD problems are approximated according to Eqs. (23), (24), and (25), respectively.



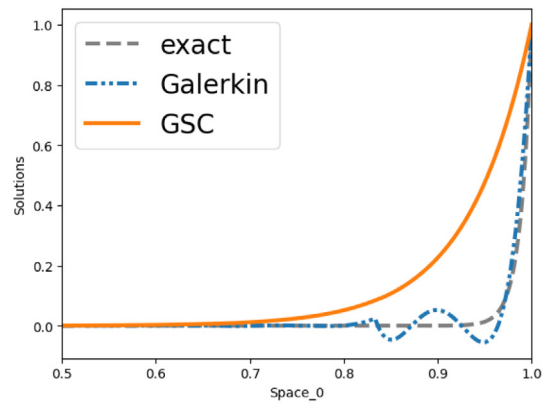
(a) AD: B-spline



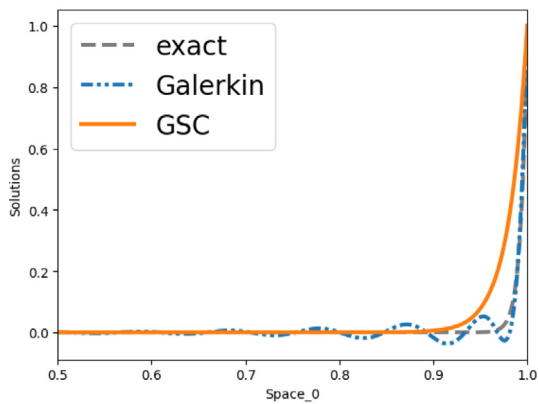
(b) AD: Lagrange



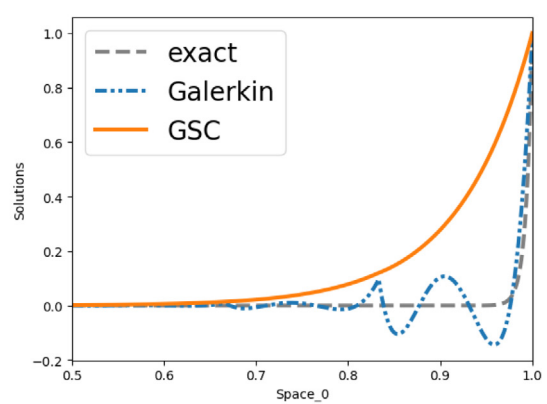
(c) RD: B-spline



(d) RD: Lagrange

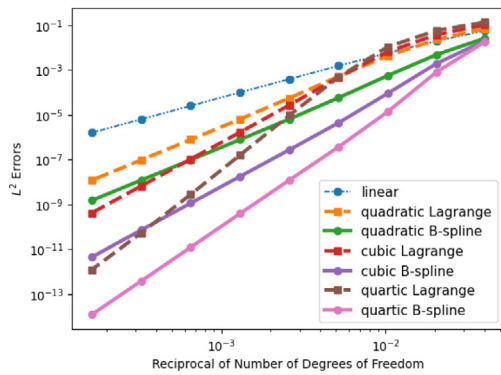


(e) ADR: B-spline

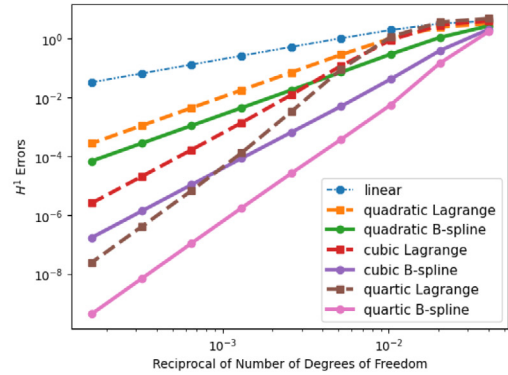


(f) ADR: Lagrange

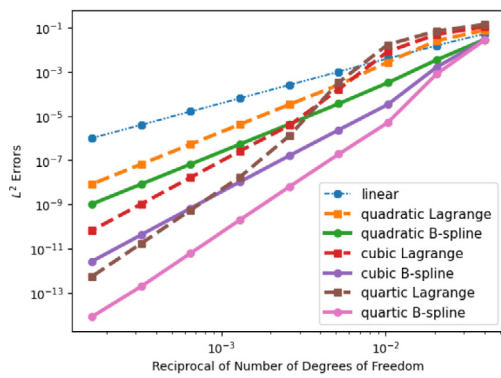
Fig. 4.11. Quartic approximate solutions computed with Galerkin and GSC methods for reactive rate $r = 7.5 \times 10^3 \text{ s}^{-1}$, advective velocity $\mathbf{a} = 1.0 \times 10^2 \text{ m s}^{-1}$, and diffusivity $\kappa = 1.0 \text{ m}^2 \text{ s}^{-1}$. The stabilization parameters for one-dimensional ADR, RD, and AD problems are approximated according to Eqs. (23), (24), and (25), respectively.



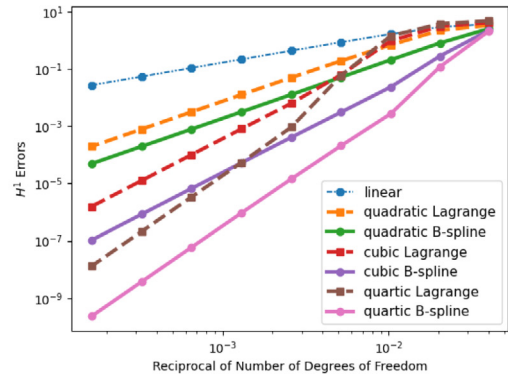
(a) AD: L^2



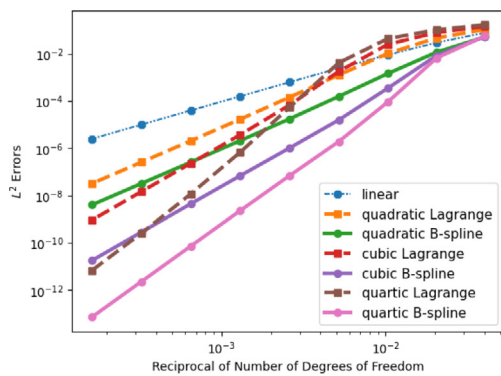
(b) AD: H^1



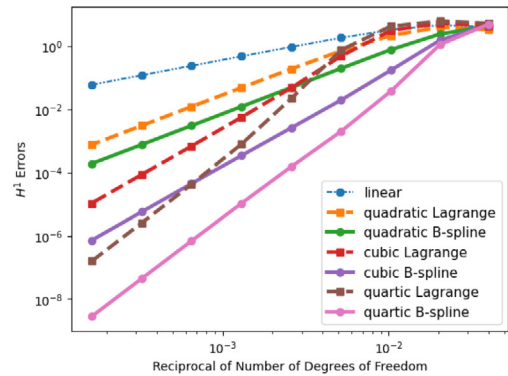
(c) RD: L^2



(d) RD: H^1



(e) ADR: L^2

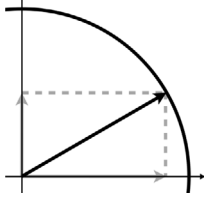


(f) ADR: H^1

Fig. 4.12. Convergence analyses (25, 49, 97, 193, 385, 769, 1537, 3073, and 6145 degrees of freedom) in the L^2 norm and H^1 semi-norm for the one-dimensional GSC method for reactive rate $r = 7.5 \times 10^3 \text{ s}^{-1}$, advective velocity $\mathbf{a} = 1.0 \times 10^2 \text{ m s}^{-1}$, and diffusivity $\kappa = 1.0 \text{ m}^2 \text{ s}^{-1}$. The stabilization parameters for one-dimensional ADR, RD, and AD problems are approximated according to Eqs. (23), (24), and (25), respectively. Corresponding convergence rates are listed in Table 4.2.

Table 5.1

Schematic representation of the streamline GSC method and its key parameters.

Streamline GSC	
	
Dimensionless numbers	$Da_h = \frac{rh^2}{\kappa}$ $Pe_h = \frac{\ \mathbf{a}\ _2 h}{\kappa}$
Reactive stabilization	$\tau_R \nabla(rw^h)$ $\tau_R = \frac{h^2}{r} \chi$ χ : Eq. (23)
Advective stabilization	$\tau_A \mathbf{a} \cdot \nabla w^h$ $\tau_A = \frac{h}{\ \mathbf{a}\ _2} \zeta$ ζ : Eq. (23)

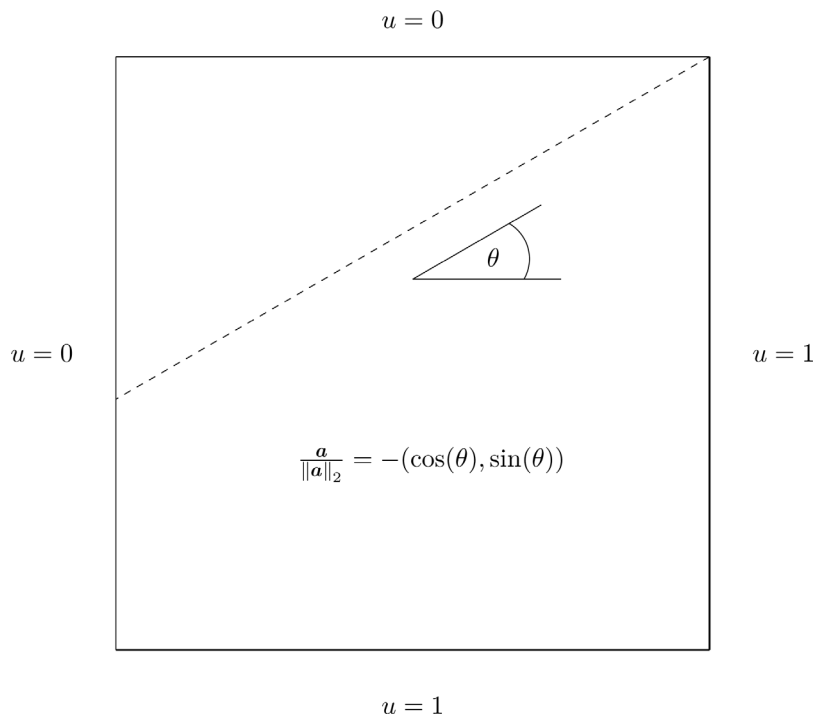


Fig. 5.1. Schematic of the Advection-Skew-to-Mesh test case.

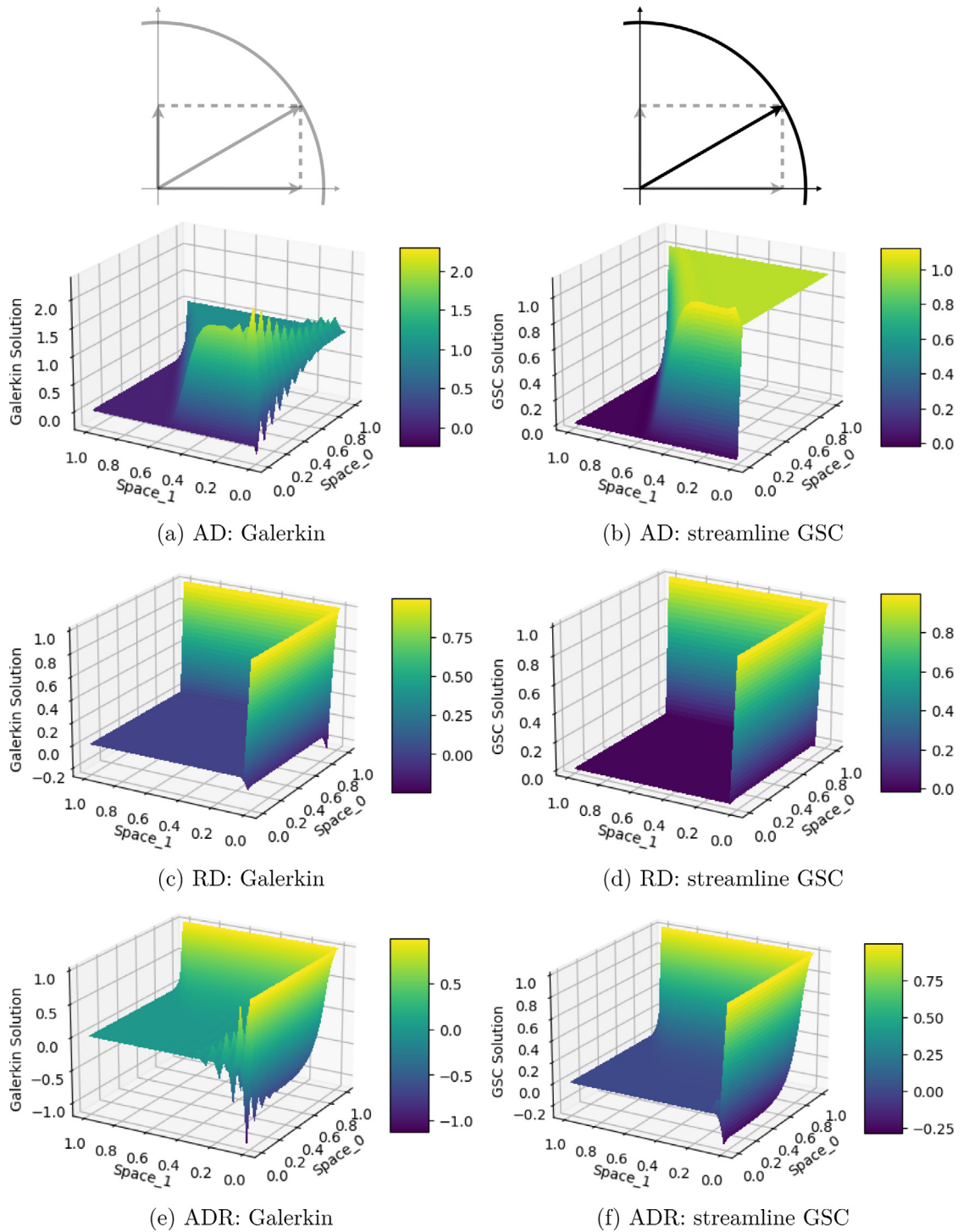


Fig. 5.2. Linear finite element solutions computed with Galerkin and streamline GSC methods for reactive rate $r = 7.5 \times 10^3 \text{ s}^{-1}$, advective velocity $\mathbf{a} = -1.0 \times 10^3 \text{ m s}^{-1} [\cos 30^\circ, \sin 30^\circ]$, and diffusivity $\kappa = 1.0 \text{ m}^2 \text{ s}^{-1}$.

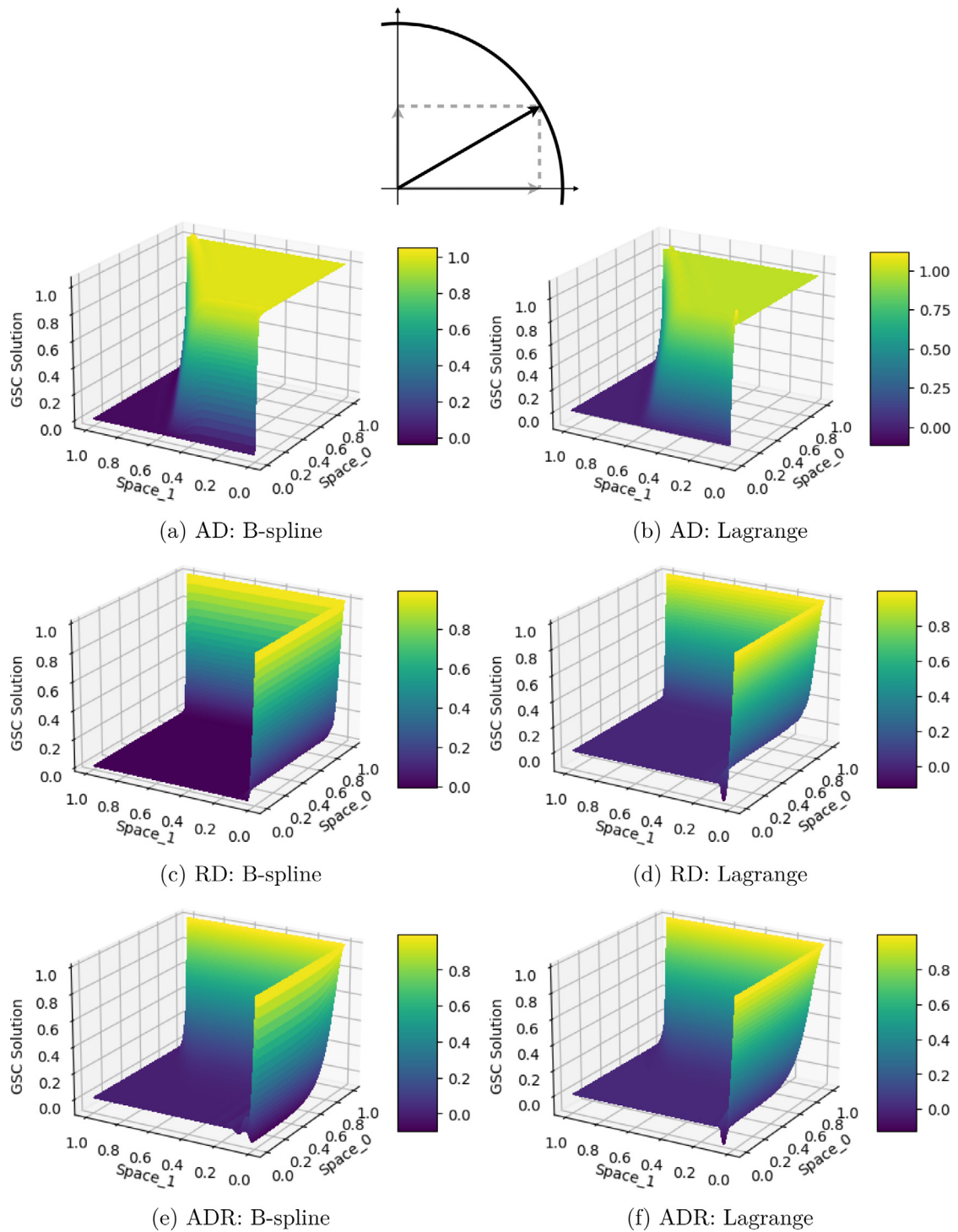


Fig. 5.3. Quadratic approximate solutions computed with the streamline GSC method for reactive rate $r = 7.5 \times 10^3 \text{ s}^{-1}$, advective velocity $\mathbf{a} = -1.0 \times 10^3 \text{ m s}^{-1} [\cos 30^\circ, \sin 30^\circ]$, and diffusivity $\kappa = 1.0 \text{ m}^2 \text{ s}^{-1}$.

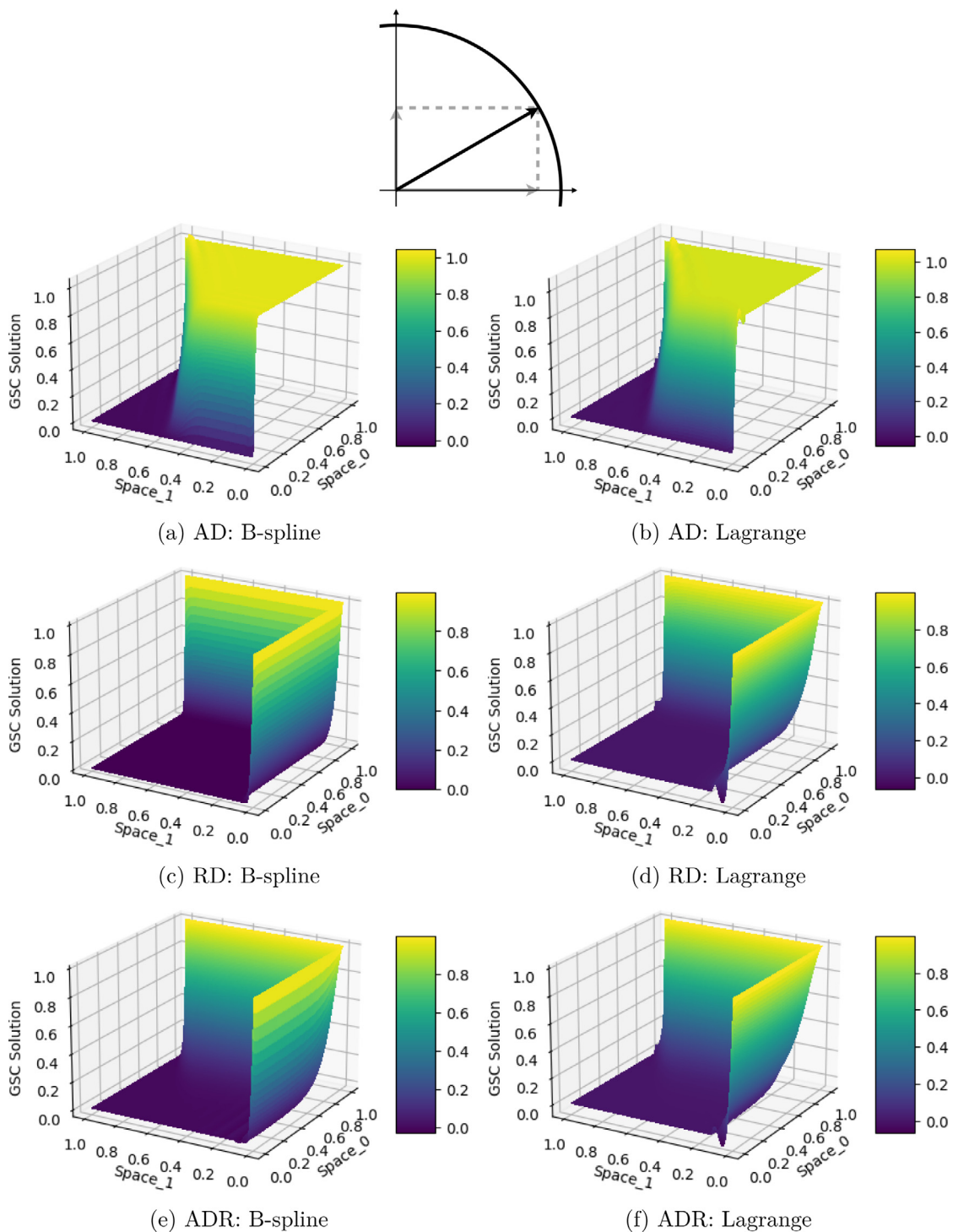


Fig. 5.4. Cubic approximate solutions computed with the streamline GSC method for reactive rate $r = 7.5 \times 10^3 \text{ s}^{-1}$, advective velocity $\mathbf{a} = -1.0 \times 10^3 \text{ m s}^{-1} [\cos 30^\circ, \sin 30^\circ]$, and diffusivity $\kappa = 1.0 \text{ m}^2 \text{ s}^{-1}$.

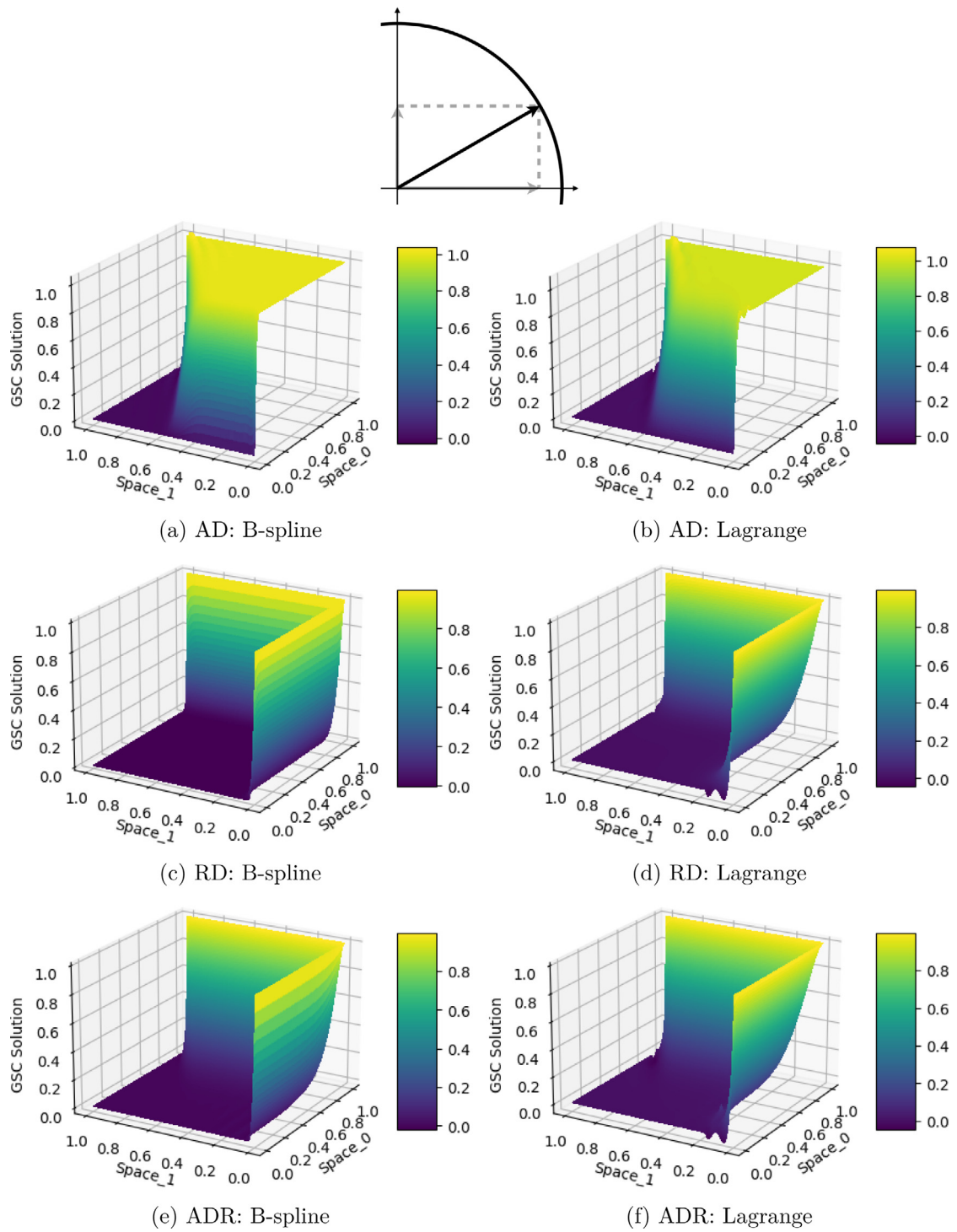
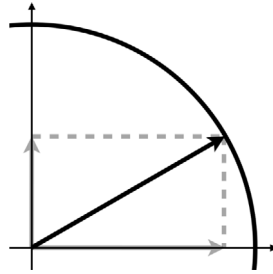


Fig. 5.5. Quartic approximate solutions computed with the streamline GSC method for reactive rate $r = 7.5 \times 10^3 \text{ s}^{-1}$, advective velocity $\mathbf{a} = -1.0 \times 10^3 \text{ m s}^{-1} [\cos 30^\circ, \sin 30^\circ]$, and diffusivity $\kappa = 1.0 \text{ m}^2 \text{ s}^{-1}$.

Table 5.2
Minimum and maximum values of the streamline GSC solutions in Figs. 5.2, 5.3, 5.4, and 5.5.



Order	Basis	AD		RD		ADR	
		min ·10 ⁻²	max	min ·10 ⁻⁴	max	min ·10 ⁻²	max
Linear	B-spline/	-1.596	1.126	-139.5	1.000	-28.85	1.000
	Lagrange						
Quadratic	B-spline	-3.184	1.052	-48.54	1.000	-9.596	1.000
	Lagrange						
Cubic	B-spline	-2.911	1.047	-2.830	1.000	-2.618	1.000
	Lagrange						
Quartic	B-spline	-2.538	1.039	-7.531	1.000	-1.728	1.000
	Lagrange						

5.1. Mathematical analysis of the streamline GSC method

Theorem 5.1. Assume

1. The terms r , \mathbf{a} , and κ are element-wise constant and h is uniform across the domain Ω .²
2. The following inverse estimates are satisfied for all $w^h \in \mathbb{V}^h$:

$$\|\nabla w^h\|_{\tilde{\Omega}}^2 \leq \frac{C_1}{h^2} \|w^h\|_{\tilde{\Omega}}^2, \tag{26}$$

$$\|\nabla \nabla w^h\|_{\tilde{\Omega}}^2 \leq \frac{C_2}{h^2} \|\nabla w^h\|_{\tilde{\Omega}}^2, \tag{27}$$

$$\|\nabla \Delta w^h\|_{\tilde{\Omega}}^2 \leq \frac{C_3}{h^2} \|\Delta w^h\|_{\tilde{\Omega}}^2. \tag{28}$$

3. There exists $\tilde{u}^h \in \mathbb{S}^h$ such that $\eta := u - \tilde{u}^h$ satisfies the estimate

$$|\eta|_{H^s(\tilde{\Omega})}^2 \leq c_{int} h^{2(k+1-s)} \|u\|_{H^{k+1}(\Omega)}^2. \tag{29}$$

4. The stabilization parameters are given by

$$\begin{aligned} \tau_R &= \frac{h^2}{r} \chi_s = \frac{h^2}{r} \frac{Da_h^2}{\alpha Da_h^2 + \beta Pe_h^2 + \gamma}, \\ \tau_A &= \frac{h}{\|\mathbf{a}\|_2} \zeta_s = \frac{h}{\|\mathbf{a}\|_2} \frac{Pe_h}{2Pe_h + 2Da_h + 4C_2} \\ &= \frac{1}{4\kappa \frac{Pe_h}{2} + \frac{Da_h}{2} + C_2} \\ &= \frac{1}{2r + \frac{2\|\mathbf{a}\|_2}{h} + \frac{4C_2\kappa}{h^2}}, \end{aligned} \tag{30}$$

where $\alpha \geq 8\sqrt{C_2 C_3}$, $\beta \geq 8C_1 C_2$, and $\gamma > 0$.

² The proof also applies to quasi-uniform mesh refinement with changes to constants.

5. The stability norm is defined as

$$\|w^h\|_{GSC}^2 := \left\| r^{\frac{1}{2}} w^h \right\|_{\tilde{\Omega}}^2 + \left\| \kappa^{\frac{1}{2}} \nabla w^h \right\|_{\tilde{\Omega}}^2 + \left\| \tau_A^{\frac{1}{2}} \mathbf{a} \cdot \nabla w^h \right\|_{\tilde{\Omega}}^2 + \left\| \tau_R^{\frac{1}{2}} r \nabla w^h \right\|_{\tilde{\Omega}}^2.$$

Then the streamline GSC method satisfies an error estimate given by

$$\|e\|_{GSC}^2 \leq \kappa C (1 + Da_h + Pe_h) \|u\|_{H^{k+1}(\Omega)}^2 h^{2k}, \tag{31}$$

where $e := u - u^h$ and the constant C depends on $C_1, C_2, C_3,$ and c_{int} .

Remark 5.2. For constant $r, \|\mathbf{a}\|_2,$ and $\kappa,$ the stability norm can be rewritten as

$$\|e\|_{GSC}^2 = \kappa \left(\frac{r}{\kappa} \|e\|_{\tilde{\Omega}}^2 + \|\nabla e\|_{\tilde{\Omega}}^2 + Pe_h \zeta_s \|\hat{\mathbf{a}} \cdot \nabla e\|_{\tilde{\Omega}}^2 + Da_h \chi_s \|\nabla e\|_{\tilde{\Omega}}^2 \right),$$

where $\mathbf{a} = \|\mathbf{a}\|_2 \hat{\mathbf{a}}$. We thus see that the left-hand side of (31) has terms of order $\mathcal{O}(Da_h)$ and $\mathcal{O}(Pe_h)$ just like the right-hand side. So, even at large element Damköhler and Péclet numbers, the bound provided by the right-hand side of (31) remains reasonably close to $\|e\|_{GSC}^2$. One might say the left-hand and right-hand sides are balanced in terms of the Damköhler and Péclet numbers. This is in contrast to the error estimate for the Galerkin method

$$\kappa \left(\frac{r}{\kappa} \|e\|_{\tilde{\Omega}}^2 + \|\nabla e\|_{\tilde{\Omega}}^2 \right) \leq \kappa C (1 + Da_h + Pe_h^2) \|u\|_{H^{k+1}(\Omega)}^2 h^{2k},$$

where only the right-hand side grows with increasing element Damköhler or Péclet number thus leading to a very poor stability and error estimate in such situations.

Remark 5.3. The choice of the stabilization parameters τ_R and τ_A in Eq. (30) builds on the approximations in Eq. (23). We note that Eq. (23) is derived for linear elements and that because $C_2 = 0$ for linear elements, the restriction on α and β is $\alpha \geq 0$ and $\beta \geq 0$. Thus the choice of $\alpha = 6, \beta = 19.2323$ and $\gamma = 216$ in Eq. (23) is valid from the point of view of Theorem 5.1. Due to the way in which χ_s is used in the ensuing lemma and proof, one can easily check that an order $\mathcal{O}(Da_h)$ term in the denominator of χ_s will have no effect on the end result. A similar line of reasoning can be applied when comparing ζ_s in Eq. (30) to ζ in Eq. (23).

Lemma 5.4 (Stability).

$$B_{GSC}^h(w^h, w^h) \geq \frac{1}{2} \|w^h\|_{GSC}^2. \tag{32}$$

Proof. We have that

$$\begin{aligned} B_{GSC}^h(w^h, w^h) &= \left\| r^{\frac{1}{2}} w^h \right\|_{\tilde{\Omega}}^2 + \left\| \kappa^{\frac{1}{2}} \nabla w^h \right\|_{\tilde{\Omega}}^2 + \left\| \tau_A^{\frac{1}{2}} \mathbf{a} \cdot \nabla w^h \right\|_{\tilde{\Omega}}^2 + \left\| \tau_R^{\frac{1}{2}} r \nabla w^h \right\|_{\tilde{\Omega}}^2 - \\ &\quad (\tau_A \mathbf{a} \cdot \nabla w^h, \kappa \Delta w^h)_{\tilde{\Omega}} + (\tau_A \mathbf{a} \cdot \nabla w^h, r w^h)_{\tilde{\Omega}} + \\ &\quad (\tau_R r \nabla w^h, \nabla(\mathbf{a} \cdot \nabla w^h))_{\tilde{\Omega}} - (\tau_R r \nabla w^h, \nabla(\kappa \Delta w^h))_{\tilde{\Omega}}. \end{aligned} \tag{33}$$

The first four terms define our stability norm $\|\cdot\|_{GSC}^2$ and our goal is to subsume the last four terms into those terms that make up the stability norm. We recall that $r, \mathbf{a},$ and κ are assumed element-wise constant.

Starting with the τ_A terms,

$$\begin{aligned} -(\tau_A \mathbf{a} \cdot \nabla w^h, r w^h)_{\tilde{\Omega}} &\geq -\frac{1}{2} \left(\frac{2}{3} \left\| \tau_A^{\frac{1}{2}} \mathbf{a} \cdot \nabla w^h \right\|_{\tilde{\Omega}}^2 + \frac{3}{2} \tau_A r \left\| r^{\frac{1}{2}} w^h \right\|_{\tilde{\Omega}}^2 \right) \\ &\geq -\frac{1}{3} \left\| \tau_A^{\frac{1}{2}} \mathbf{a} \cdot \nabla w^h \right\|_{\tilde{\Omega}}^2 - \frac{3}{8} \left\| r^{\frac{1}{2}} w^h \right\|_{\tilde{\Omega}}^2. \end{aligned}$$

with the last step taking advantage of the fact that $\tau_A \leq \frac{1}{2r}$. Likewise,

$$\begin{aligned} -(\tau_A \mathbf{a} \cdot \nabla w^h, \kappa \Delta w^h)_{\tilde{\Omega}} &\geq -\frac{1}{2} \left(\frac{1}{3} \left\| \tau_A^{\frac{1}{2}} \mathbf{a} \cdot \nabla w^h \right\|_{\tilde{\Omega}}^2 + 3\tau_A \kappa \left\| \kappa^{\frac{1}{2}} \Delta w^h \right\|_{\tilde{\Omega}}^2 \right) \\ &\geq -\frac{1}{2} \left(\frac{1}{3} \left\| \tau_A^{\frac{1}{2}} \mathbf{a} \cdot \nabla w^h \right\|_{\tilde{\Omega}}^2 + \frac{3\tau_A \kappa C_2}{h^2} \left\| \kappa^{\frac{1}{2}} \nabla w^h \right\|_{\tilde{\Omega}}^2 \right) \\ &\geq -\frac{1}{6} \left\| \tau_A^{\frac{1}{2}} \mathbf{a} \cdot \nabla w^h \right\|_{\tilde{\Omega}}^2 - \frac{3}{8} \left\| \kappa^{\frac{1}{2}} \nabla w^h \right\|_{\tilde{\Omega}}^2, \end{aligned}$$

where the very last inequality takes advantage of the fact that $\tau_A \leq \frac{h^2}{4C_2\kappa}$.

For the τ_R terms, a bit more detail is required:

$$\begin{aligned} (\tau_R r \nabla w^h, \nabla(\mathbf{a} \cdot \nabla w^h))_{\tilde{\Omega}} &\geq -\frac{1}{4} \left\| \tau_R^{\frac{1}{2}} r \nabla w^h \right\|_{\tilde{\Omega}}^2 - \left\| \tau_R^{\frac{1}{2}} \mathbf{a} \cdot \nabla \nabla w^h \right\|_{\tilde{\Omega}}^2 \quad \left(\text{Peter-Paul with } \varepsilon = \frac{1}{2} \right) \\ &\geq -\frac{1}{4} \left\| \tau_R^{\frac{1}{2}} r \nabla w^h \right\|_{\tilde{\Omega}}^2 - \tau_R \|\mathbf{a}\|_2^2 \frac{C_2}{h^2} \left\| \nabla w^h \right\|_{\tilde{\Omega}}^2 \quad \left(\text{using Eq. (27)} \right) \\ &\geq -\frac{1}{4} \left\| \tau_R^{\frac{1}{2}} r \nabla w^h \right\|_{\tilde{\Omega}}^2 - \tau_R \|\mathbf{a}\|_2^2 \frac{C_2 C_1}{r h^4} \left\| r^{\frac{1}{2}} w^h \right\|_{\tilde{\Omega}}^2 \quad \left(\text{using Eq. (26)} \right) \\ &\geq -\frac{1}{4} \left\| \tau_R^{\frac{1}{2}} r \nabla w^h \right\|_{\tilde{\Omega}}^2 - C_1 C_2 \frac{P e_h^2}{D a_h^2} \chi_s \left\| r^{\frac{1}{2}} w^h \right\|_{\tilde{\Omega}}^2 \quad \left(\text{using } \frac{\|\mathbf{a}\|_2^2 h^2}{r^2 h^4} = \frac{P e_h^2}{D a_h^2} \right) \\ &\geq -\frac{1}{4} \left\| \tau_R^{\frac{1}{2}} r \nabla w^h \right\|_{\tilde{\Omega}}^2 - \frac{C_1 C_2}{\beta} \left\| r^{\frac{1}{2}} w^h \right\|_{\tilde{\Omega}}^2 \quad \left(\text{using } \frac{P e_h^2}{\alpha D a_h^2 + \beta P e_h^2 + \gamma} \leq \frac{1}{\beta} \right) \\ &\geq -\frac{1}{4} \left\| \tau_R^{\frac{1}{2}} r \nabla w^h \right\|_{\tilde{\Omega}}^2 - \frac{1}{8} \left\| r^{\frac{1}{2}} w^h \right\|_{\tilde{\Omega}}^2. \end{aligned}$$

The last line is true provided that

$$\beta \geq 8C_1 C_2.$$

The last term becomes

$$\begin{aligned} -(\tau_R r \nabla w^h, \nabla(\kappa \Delta w^h))_{\tilde{\Omega}} &\geq -\frac{1}{16} \left\| \kappa^{\frac{1}{2}} \nabla w^h \right\|_{\tilde{\Omega}}^2 - 4\tau_R^2 r^2 \left\| \kappa^{\frac{1}{2}} \nabla \Delta w^h \right\|_{\tilde{\Omega}}^2 \quad \left(\text{Peter-Paul with } \varepsilon = \frac{1}{8} \right) \\ &\geq -\frac{1}{16} \left\| \kappa^{\frac{1}{2}} \nabla w^h \right\|_{\tilde{\Omega}}^2 - 4\tau_R^2 r^2 \frac{C_3 C_2}{h^4} \left\| \kappa^{\frac{1}{2}} \nabla w^h \right\|_{\tilde{\Omega}}^2 \quad \left(\text{Eqs. (28) and (27)} \right) \\ &\geq -\frac{1}{16} \left\| \kappa^{\frac{1}{2}} \nabla w^h \right\|_{\tilde{\Omega}}^2 - 4C_2 C_3 \chi_s^2 \left\| \kappa^{\frac{1}{2}} \nabla w^h \right\|_{\tilde{\Omega}}^2 \\ &\geq -\frac{1}{16} \left\| \kappa^{\frac{1}{2}} \nabla w^h \right\|_{\tilde{\Omega}}^2 - \frac{4C_2 C_3}{\alpha^2} \left\| \kappa^{\frac{1}{2}} \nabla w^h \right\|_{\tilde{\Omega}}^2 \quad \left(\text{using } \chi_s \leq \frac{1}{\alpha} \right) \\ &\geq -\frac{1}{16} \left\| \kappa^{\frac{1}{2}} \nabla w^h \right\|_{\tilde{\Omega}}^2 - \frac{1}{16} \left\| \kappa^{\frac{1}{2}} \nabla w^h \right\|_{\tilde{\Omega}}^2 \end{aligned}$$

provided $\alpha \geq 8\sqrt{C_2 C_3}$.

As such the choice of suitable α and β ensures that the method is coercive with

$$B_{\text{GSC}}^h(w^h, w^h) \geq \frac{1}{2} \|w^h\|_{\text{GSC}}^2. \quad \square$$

Proof of Theorem 5.1. We first note that the error $e = u - u^h$ can be decomposed into the interpolation error $\eta = u - \tilde{u}^h$, which measures how well the solution space can approximate the exact solution, and the numerical method error $e^h := (\tilde{u}^h - u^h) \in \mathbb{V}^h$, which measures how well the method approximates the best-fit interpolate. We will prove the error estimates for e^h and η separately. Starting with e^h , we make use of stability (32) along with

Galerkin orthogonality to get

$$\begin{aligned} \frac{1}{2} \|e^h\|_{\text{GSC}}^2 &\leq |B_{\text{GSC}}^h(e^h, \eta)| \\ &\leq |(re^h, \eta)_{\tilde{\Omega}}| + |(\mathbf{a} \cdot \nabla e^h, \eta)_{\tilde{\Omega}}| + |(\kappa \nabla e^h, \nabla \eta)_{\tilde{\Omega}}| + |(\tau_A \mathbf{a} \cdot \nabla e^h, r\eta)_{\tilde{\Omega}}| \\ &\quad + |(\tau_A \mathbf{a} \cdot \nabla e^h, \mathbf{a} \cdot \nabla \eta)_{\tilde{\Omega}}| + |(\tau_A \mathbf{a} \cdot \nabla e^h, \kappa \Delta \eta)_{\tilde{\Omega}}| + |(\tau_R r \nabla e^h, r \nabla \eta)_{\tilde{\Omega}}| \\ &\quad + |(\tau_R r \nabla e^h, \nabla(\mathbf{a} \cdot \nabla \eta))_{\tilde{\Omega}}| + |(\tau_R r \nabla e^h, \nabla(\kappa \Delta \eta))_{\tilde{\Omega}}|. \end{aligned}$$

Using Cauchy–Schwarz and the Peter-Paul inequalities we obtain

$$\begin{aligned} \frac{1}{2} \|e^h\|_{\text{GSC}}^2 &\leq \frac{1}{2} \left(\varepsilon_1 \|r^{\frac{1}{2}} e^h\|_{\tilde{\Omega}}^2 + (\varepsilon_2 + \varepsilon_4 + \varepsilon_5 + \varepsilon_6) \left\| \tau_A^{\frac{1}{2}} \mathbf{a} \cdot \nabla e^h \right\|_{\tilde{\Omega}}^2 + (\varepsilon_3 + \varepsilon_9) \left\| \kappa^{\frac{1}{2}} \nabla e^h \right\|_{\tilde{\Omega}}^2 \right. \\ &\quad + (\varepsilon_7 + \varepsilon_8) \left\| \tau_R^{\frac{1}{2}} r \nabla e^h \right\|_{\tilde{\Omega}}^2 + \varepsilon_1^{-1} \|r^{\frac{1}{2}} \eta\|_{\tilde{\Omega}}^2 + \varepsilon_2^{-1} \left\| \tau_A^{-\frac{1}{2}} \eta \right\|_{\tilde{\Omega}}^2 \\ &\quad + \varepsilon_3^{-1} \left\| \kappa^{\frac{1}{2}} \nabla \eta \right\|_{\tilde{\Omega}}^2 + \varepsilon_4^{-1} \left\| \tau_A^{\frac{1}{2}} r \eta \right\|_{\tilde{\Omega}}^2 + \varepsilon_5^{-1} \left\| \tau_A^{\frac{1}{2}} \mathbf{a} \cdot \nabla \eta \right\|_{\tilde{\Omega}}^2 \\ &\quad + \varepsilon_6^{-1} \left\| \tau_A^{\frac{1}{2}} \kappa \Delta \eta \right\|_{\tilde{\Omega}}^2 + \varepsilon_7^{-1} \left\| \tau_R^{\frac{1}{2}} r \nabla \eta \right\|_{\tilde{\Omega}}^2 \\ &\quad \left. + \varepsilon_8^{-1} \left\| \tau_R^{\frac{1}{2}} \nabla(\mathbf{a} \cdot \nabla \eta) \right\|_{\tilde{\Omega}}^2 + \varepsilon_9^{-1} \left\| \tau_R r \kappa^{\frac{1}{2}} \nabla \Delta \eta \right\|_{\tilde{\Omega}}^2 \right). \end{aligned}$$

We then let $\varepsilon_1 = \frac{1}{2}$, $\varepsilon_2 = \varepsilon_4 = \varepsilon_5 = \varepsilon_6 = \frac{1}{8}$ and $\varepsilon_7 = \varepsilon_8 = \varepsilon_3 = \varepsilon_9 = \frac{1}{4}$ to get

$$\begin{aligned} \|e^h\|_{\text{GSC}}^2 &\leq C \left(\left\| \kappa^{\frac{1}{2}} \nabla \eta \right\|_{\tilde{\Omega}}^2 + \|r^{\frac{1}{2}} \eta\|_{\tilde{\Omega}}^2 + \left\| \tau_A^{-\frac{1}{2}} \eta \right\|_{\tilde{\Omega}}^2 + \left\| \tau_A^{\frac{1}{2}} r \eta \right\|_{\tilde{\Omega}}^2 + \left\| \tau_A^{\frac{1}{2}} \mathbf{a} \cdot \nabla \eta \right\|_{\tilde{\Omega}}^2 + \left\| \tau_A^{\frac{1}{2}} \kappa \Delta \eta \right\|_{\tilde{\Omega}}^2 \right. \\ &\quad \left. + \left\| \tau_R^{\frac{1}{2}} r \nabla \eta \right\|_{\tilde{\Omega}}^2 + \left\| \tau_R^{\frac{1}{2}} \nabla(\mathbf{a} \cdot \nabla \eta) \right\|_{\tilde{\Omega}}^2 + \left\| r \tau_R \kappa^{\frac{1}{2}} \nabla \Delta \eta \right\|_{\tilde{\Omega}}^2 \right). \end{aligned}$$

We go through each of the τ_A and τ_R terms to determine their convergence rates.

$$\left\| \tau_A^{-\frac{1}{2}} \eta \right\|_{\tilde{\Omega}}^2$$

From Eq. (30), we have that

$$\tau_A \geq \frac{h^2}{4\kappa} \frac{1}{3 \max \left\{ \frac{Pe_h}{2}, \frac{Da_h}{2}, C_2 \right\}}.$$

Thus

$$\begin{aligned} \left\| \tau_A^{-\frac{1}{2}} \eta \right\|_{\tilde{\Omega}}^2 &\leq \frac{12\kappa}{h^2} \max \left\{ \frac{Pe_h}{2}, \frac{Da_h}{2}, C_2 \right\} c_{int} h^{2(k+1)} \|u\|_{H^{k+1}(\Omega)}^2 \\ &\leq \left(12 c_{int} \kappa \max \left\{ \frac{Pe_h}{2}, \frac{Da_h}{2}, C_2 \right\} \right) \|u\|_{H^{k+1}(\Omega)}^2 h^{2k}. \end{aligned}$$

$$\left\| \tau_A^{\frac{1}{2}} r \eta \right\|_{\tilde{\Omega}}^2$$

Note that $\tau_A \leq \min \left\{ \frac{1}{2r}, \frac{h}{2\|\mathbf{a}\|_2}, \frac{h^2}{4C_2\kappa} \right\}$. In particular, $\tau_A \leq \frac{1}{2r}$ and thus

$$\begin{aligned} \left\| \tau_A^{\frac{1}{2}} r \eta \right\|_{\tilde{\Omega}}^2 &\leq c_{int} \frac{r}{2} \|u\|_{H^{k+1}(\Omega)}^2 h^{2(k+1)} \\ &\leq \frac{Da_h c_{int} \kappa}{2} \|u\|_{H^{k+1}(\Omega)}^2 h^{2k}. \end{aligned}$$

$$\begin{aligned} & \left\| \tau_A^{\frac{1}{2}} \mathbf{a} \cdot \nabla \eta \right\|_{\tilde{\Omega}}^2 \\ & \text{Because } \tau_A \leq \frac{h}{2\|\mathbf{a}\|_2} \\ & \left\| \tau_A^{\frac{1}{2}} \mathbf{a} \cdot \nabla \eta \right\|_{\tilde{\Omega}}^2 \leq \tau_A \|\mathbf{a}\|_2^2 \|\nabla \eta\|_{\tilde{\Omega}}^2 \\ & \leq \underbrace{\frac{\|\mathbf{a}\|_2 h}{2\kappa}}_{\frac{Pe_h}{2}} \kappa \|\nabla \eta\|_{\tilde{\Omega}}^2 \\ & \leq c_{int} \kappa \frac{Pe_h}{2} \|u\|_{H^{k+1}(\Omega)}^2 h^{2k}. \end{aligned}$$

$$\begin{aligned} & \left\| \tau_A^{\frac{1}{2}} \kappa \Delta \eta \right\|_{\tilde{\Omega}}^2 \\ & \text{We use } \tau_A \leq \frac{h^2}{4C_2\kappa} \\ & \left\| \tau_A^{\frac{1}{2}} \kappa \Delta \eta \right\|_{\tilde{\Omega}}^2 \leq \frac{h^2}{4C_2\kappa} \kappa^2 \|\Delta \eta\|_{\tilde{\Omega}}^2 \\ & \leq \frac{c_{int}\kappa}{4C_2} \|u\|_{H^{k+1}(\Omega)}^2 h^{2k}. \end{aligned}$$

$$\begin{aligned} & \left\| \tau_R^{\frac{1}{2}} r \nabla \eta \right\|_{\tilde{\Omega}}^2 \\ & \left\| \tau_R^{\frac{1}{2}} r \nabla \eta \right\|_{\tilde{\Omega}}^2 = \frac{rh^2}{\kappa} \kappa \chi_s \|\nabla \eta\|_{\tilde{\Omega}}^2 \\ & \leq \kappa \frac{Da_h}{\alpha} c_{int} \|u\|_{H^{k+1}(\Omega)}^2 h^{2k}. \end{aligned}$$

For the second line, we use the fact that $\chi_s \leq \frac{1}{\alpha}$.

$$\begin{aligned} & \left\| \tau_R^{\frac{1}{2}} \nabla(\mathbf{a} \cdot \nabla \eta) \right\|_{\tilde{\Omega}}^2 \\ & \left\| \tau_R^{\frac{1}{2}} \nabla(\mathbf{a} \cdot \nabla \eta) \right\|_{\tilde{\Omega}}^2 \leq \tau_R \|\mathbf{a}\|_2^2 \|\nabla \nabla \eta\|_{\tilde{\Omega}}^2 \\ & = \frac{h^2}{r} \chi_s \|\mathbf{a}\|_2^2 \|\nabla \nabla \eta\|_{\tilde{\Omega}}^2 \\ & = \kappa \frac{Pe_h^2 Da_h}{\alpha Da_h^2 + \beta Pe_h^2 + \gamma} h^2 \|\nabla \nabla \eta\|_{\tilde{\Omega}}^2. \end{aligned}$$

Because $\frac{Pe_h^2 Da_h}{\alpha Da_h^2 + \beta Pe_h^2 + \gamma} \leq \frac{Da_h}{\beta}$, we then have that

$$\begin{aligned} & \left\| \tau_R^{\frac{1}{2}} \nabla(\mathbf{a} \cdot \nabla \eta) \right\|_{\tilde{\Omega}}^2 \leq \kappa \frac{Da_h}{\beta} h^2 \|\nabla \nabla \eta\|_{\tilde{\Omega}}^2 \\ & \leq \frac{Da_h}{\beta^2} \kappa c_{int} \|u\|_{H^{k+1}(\Omega)}^2 h^{2k}. \end{aligned}$$

$$\begin{aligned} & \left\| r \tau_R \kappa^{\frac{1}{2}} \nabla \Delta \eta \right\|_{\tilde{\Omega}}^2 \\ & \left\| r \tau_R \kappa^{\frac{1}{2}} \nabla \Delta \eta \right\|_{\tilde{\Omega}}^2 = \kappa r^2 \tau_R^2 \|\nabla \Delta \eta\|_{\tilde{\Omega}}^2 \end{aligned}$$

$$\begin{aligned}
 &= \kappa \chi_s^2 h^4 \|\nabla \Delta \eta\|_{\tilde{\Omega}}^2 \\
 &\leq \frac{c_{int} \kappa}{\alpha^2} \|u\|_{H^{k+1}(\Omega)}^2 h^{2k},
 \end{aligned}$$

where we used the fact that $\chi_s \leq \frac{1}{\alpha}$ in the last step.

To complete the proof, we collect results

$$\|\eta\|_{\text{GSC}}^2 = \left\| r^{\frac{1}{2}} \eta \right\|_{\tilde{\Omega}}^2 + \left\| \kappa^{\frac{1}{2}} \nabla \eta \right\|_{\tilde{\Omega}}^2 + \left\| \tau_A^{\frac{1}{2}} \mathbf{a} \cdot \nabla \eta \right\|_{\tilde{\Omega}}^2 + \left\| \tau_R^{\frac{1}{2}} r \nabla \eta \right\|_{\tilde{\Omega}}^2,$$

$$\begin{aligned}
 \left\| r^{\frac{1}{2}} \eta \right\|_{\tilde{\Omega}}^2 &\leq \kappa c_{int} Da_h \|u\|_{H^{k+1}(\Omega)}^2 h^{2k}, \\
 \left\| \kappa^{\frac{1}{2}} \nabla \eta \right\|_{\tilde{\Omega}}^2 &\leq \kappa c_{int} \|u\|_{H^{k+1}(\Omega)}^2 h^{2k}, \\
 \left\| \tau_A^{\frac{1}{2}} \mathbf{a} \cdot \nabla \eta \right\|_{\tilde{\Omega}}^2 &\leq \kappa c_{int} Pe_h \|u\|_{H^{k+1}(\Omega)}^2 h^{2k}, \\
 \left\| \tau_R^{\frac{1}{2}} r \nabla \eta \right\|_{\tilde{\Omega}}^2 &\leq \kappa c_{int} Da_h \|u\|_{H^{k+1}(\Omega)}^2 h^{2k}.
 \end{aligned}$$

Combining all the above inequalities we have shown that

$$\|e^h + \eta\|_{\text{GSC}}^2 \leq \kappa C (1 + Da_h + Pe_h) \|u\|_{H^{k+1}(\Omega)}^2 h^{2k}. \quad \square$$

6. Directional GSC method

We have found that results are improved by a variant of the GSC method that we refer to as the **Directional GSC Method**,

$$\begin{aligned}
 B_{\text{GSC}}^h(u^h, w^h) &= B^h(u^h, w^h) + (\tau_R \nabla(rw^h), \nabla \mathcal{L}u^h)_{\tilde{\Omega}} + (\tau_A \mathbf{a} \cdot \nabla w^h, \mathcal{L}u^h)_{\tilde{\Omega}}, \\
 L_{\text{GSC}}^h(w^h) &= L^h(w^h) + (\tau_R \nabla(rw^h), \nabla f)_{\tilde{\Omega}} + (\tau_A \mathbf{a} \cdot \nabla w^h, f)_{\tilde{\Omega}}.
 \end{aligned}$$

Note that τ_R and τ_A are now square matrices and the streamline GSC method is obtained for $\tau_R = \tau_R \mathbf{I}$ and $\tau_A = \tau_A \mathbf{I}$ (where \mathbf{I} denotes the d -dimensional identity matrix, d being the spatial dimension). In contrast, the directional GSC method computes stabilization parameters based on the element principal axes. One approach to define such principal axes $\tilde{\mathbf{e}}_i$ is presented in [Appendix B](#) for two-dimensional problems. Accordingly, changing from Euclidean axes \mathbf{e}_i is achieved by inverting the orthogonal change-of-basis matrix $\mathbf{T}_{\tilde{\mathbf{I}}}$, e.g., for the advective velocity \mathbf{a} :

$$\tilde{\mathbf{a}} = \mathbf{T}_{\tilde{\mathbf{I}}}^T \mathbf{a}.$$

The transformed components $\tilde{\mathbf{a}}^i$ of the advective velocity are then used to define the element Péclet numbers with respect to the principal axes

$$\tilde{Pe}_h^i = \frac{\tilde{\mathbf{a}}^i h}{\kappa}.$$

Next, diagonal stabilization matrices are determined and subsequently transformed from the principal to Euclidean axes

$$\tau_R = \mathbf{T}_{\tilde{\mathbf{I}}} \text{diag} \left(\frac{h^2}{r} \tilde{\chi}^i \right) \mathbf{T}_{\tilde{\mathbf{I}}}^T \quad \text{and} \quad \tau_A = \mathbf{T}_{\tilde{\mathbf{I}}} \text{diag} \left(\frac{h}{\tilde{\mathbf{a}}^i} \tilde{\zeta}^i \right) \mathbf{T}_{\tilde{\mathbf{I}}}^T.$$

The directional and streamline GSC methods are schematically illustrated and compared in [Table 6.1](#). The black arrows in the diagram of the GSC method represents the transformed velocity components $\tilde{\mathbf{a}}^i$ and indicate that the stabilization is performed along the element principal axes. We note that in all our computations, the element principal axes are aligned with the global coordinate axes.

We consider the Advection-Skew-to-Mesh problem (see [Fig. 5.1](#)) for the directional GSC method using the approximate stabilization parameters for all cases. Numerical results for the linear finite element solutions of the

Table 6.1
Schematic representation of the streamline and directional GSC methods and their key parameters.

	Streamline	Directional
Dimensionless numbers	$Da_h = \frac{r h^2}{\kappa}$ $Pe_h = \frac{\ \mathbf{a}\ _2 h}{\kappa}$	$\tilde{P}e_h^i = \frac{\tilde{\mathbf{a}}^i h}{\kappa}$
Reactive stabilization	$\tau_R \nabla(r w^h)$ $\tau_R = \frac{h^2}{r} \chi$ χ : Eq. (23)	$\tau_R \nabla(r w^h)$ $\tau_R = \mathbf{T}_I \text{diag} \left(\frac{h^2}{r} \tilde{\chi}^i \right) \mathbf{T}_I^T$ $\tilde{\chi}^i$: Eq. (23) with Pe_h replaced by $\tilde{P}e_h^i$
Advective stabilization	$\tau_A \mathbf{a} \cdot \nabla w^h$ $\tau_A = \frac{h}{\ \mathbf{a}\ _2} \zeta$ ζ : Eq. (23)	$\tau_A \mathbf{a} \cdot \nabla w^h$ $\tau_A = \mathbf{T}_I \text{diag} \left(\frac{h}{\tilde{\mathbf{a}}^i} \tilde{\zeta}^i \right) \mathbf{T}_I^T$ $\tilde{\zeta}^i$: Eq. (23) with Pe_h replaced by $\tilde{P}e_h^i$

two GSC methods are presented in Fig. 6.1. The quadratic, cubic, and quartic B-spline and Lagrange solutions for the directional GSC method are presented in Figs. 6.2, 6.3, and 6.4, respectively. In all these simulations, we use 625 degrees of freedom to solve the problem. The directional GSC method better captures the different interactions between reaction and the advective velocity components corresponding to the direction of flow when compared to the streamline GSC method. The minimum and maximum values for the AD and ADR problems are listed in Table 6.2 and a comparison to Table 5.2 shows that the directional GSC method performs either about the same as the streamline GSC method or improves upon it.³ Note that the minima and maxima for B-spline elements are always smaller in magnitude than those for Lagrange elements.

6.1. Advection in a rotating flow field

The advective velocity is proportional to $[0.5 - \mathbf{x}_1, \mathbf{x}_0 - 0.5]$ and leads to the rotation of a $\sin^2[2\pi(\mathbf{x}_0 - 0.5)]$ hill-like profile for $\mathbf{x}_0 \in [0.5, 1]$, $\mathbf{x}_1 = 0.5$ about the center of the unit square with homogeneous Dirichlet boundary conditions. The domain is composed of four patches and the profile is enforced by means of a Dirichlet boundary condition at the slit between the first and fourth quadrant of the square (see Fig. 6.5). Results for the directional GSC method using 625 degrees of freedom are reported in Fig. 6.6. This is a test of accuracy rather than stability of the method. All results are very accurate, and essentially similar to the streamline GSC method, which for this case ($r = 0$) reduces to the classical SUPG method. This shows that the directional GSC method maintains the accuracy of the streamline method in situations with a variable direction of flow.

6.2. Numerical stability analysis of the directional GSC method

We perform a numerical *inf-sup* stability analysis of the directional GSC method for the AD problem:

$$\begin{aligned} \mathbf{a} \cdot \nabla u - \kappa \Delta u &= f, & x \in \Omega, \\ u &= g, & x \in \Gamma. \end{aligned}$$

³ The minima of the Lagrange element solutions result from interpolating the discontinuous boundary conditions in the corners and are thus the same for both methods.

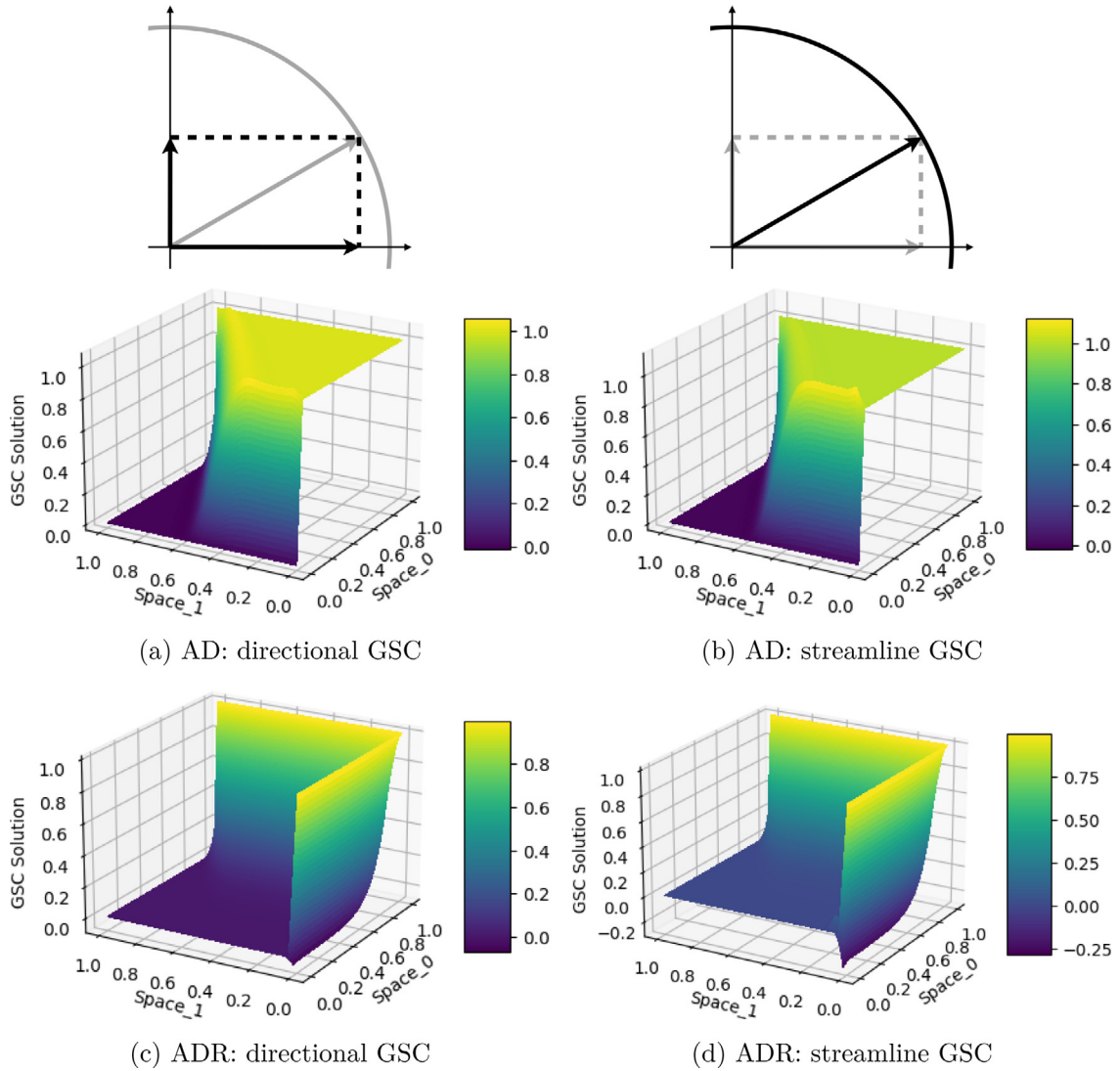


Fig. 6.1. Linear finite element solutions computed with directional and streamline GSC methods for reactive rate $r = 7.5 \times 10^3 \text{ s}^{-1}$, advective velocity $\mathbf{a} = -1.0 \times 10^3 \text{ m s}^{-1} [\cos 30^\circ, \sin 30^\circ]$, and diffusivity $\kappa = 1.0 \text{ m}^2 \text{ s}^{-1}$.

The directional GSC method takes the form

$$B_{\text{GSC}}^h(u^h, w^h) = B^h(u^h, w^h) + (\tau_A \mathbf{a} \cdot \nabla w^h, \mathcal{L}u^h)_{\tilde{\Omega}},$$

$$L_{\text{GSC}}^h(w^h) = L^h(w^h) + (\tau_A \mathbf{a} \cdot \nabla w^h, f)_{\tilde{\Omega}}.$$

With the definition

$$\mathbf{A} = (\tau_A \mathbf{a}) \otimes \mathbf{a}$$

one can show that there exists a vector $\mathbf{y} \in \mathbb{R}^d$ such that $\mathbf{y}^T \cdot \mathbf{A} \cdot \mathbf{y} < 0$. This demonstrates the bilinear form for advection-dominant problem is not coercive.

Given a bilinear form $B(\cdot, \cdot)$ and some norms $\|\cdot\|_{\text{Stab}}$ and $\|\|\cdot\|\|$ defined on a test space \mathbb{V} and its discrete counterpart $\mathbb{V}^h \subset \mathbb{V}$ such that

$$B(w^h, v) \leq C \|w^h\|_{\text{Stab}} \|v\| \quad \text{for all } v \in \mathbb{V}, w^h \in \mathbb{V}^h, \tag{Boundedness} \tag{34}$$

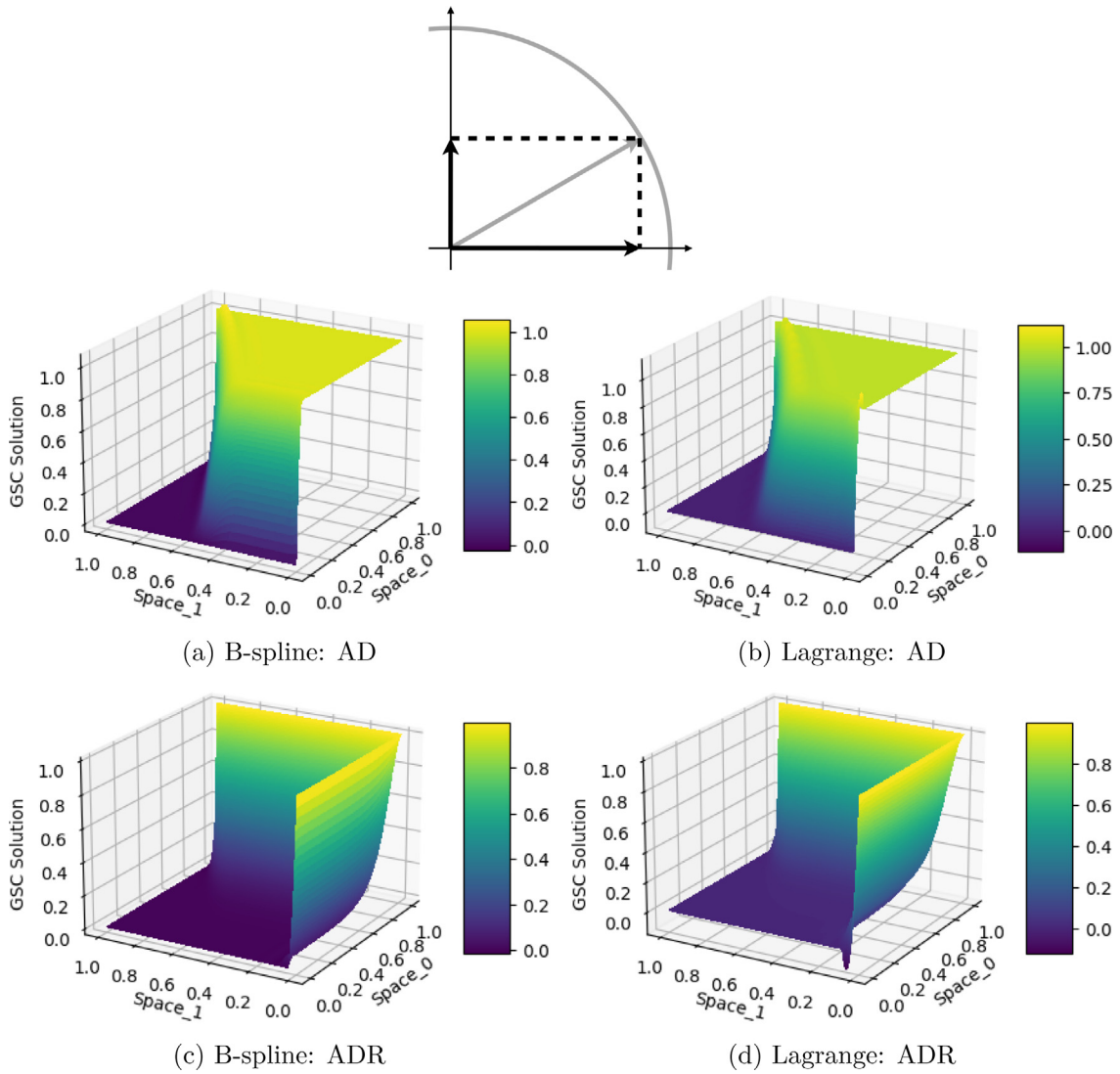


Fig. 6.2. Quadratic approximate solutions computed with the directional GSC method for reactive rate $r = 7.5 \times 10^3 \text{ s}^{-1}$, advective velocity $\mathbf{a} = -1.0 \times 10^3 \text{ m s}^{-1} [\cos 30^\circ, \sin 30^\circ]$, and diffusivity $\kappa = 1.0 \text{ m}^2 \text{ s}^{-1}$.

$$\inf_{v^h \in \mathbb{V}^h} \sup_{w^h \in \mathbb{V}^h} \frac{B(w^h, v^h)}{\|w^h\|_{\text{Stab}} \|v^h\|_{\text{Stab}}} \geq \gamma > 0, \tag{inf - sup stability} \tag{35}$$

one can show that

$$\|u - u^h\|_{\text{Stab}} \leq \|\eta\|_{\text{Stab}} + \frac{C}{\gamma} \|\eta\|, \tag{36}$$

where η is the interpolation error for the discrete test space \mathbb{V}^h .

We show *inf-sup* stability numerically following the method outlined by Bathe et al. [22]. We shall compare the *inf-sup* constants produced by the directional GSC method, the streamline GSC method (i.e., SUPG since $r = 0$), and the unstabilized Galerkin method. Given a basis $\{w_A\} \subset \mathbb{V}^h$ defined on rectangular elements, we can define

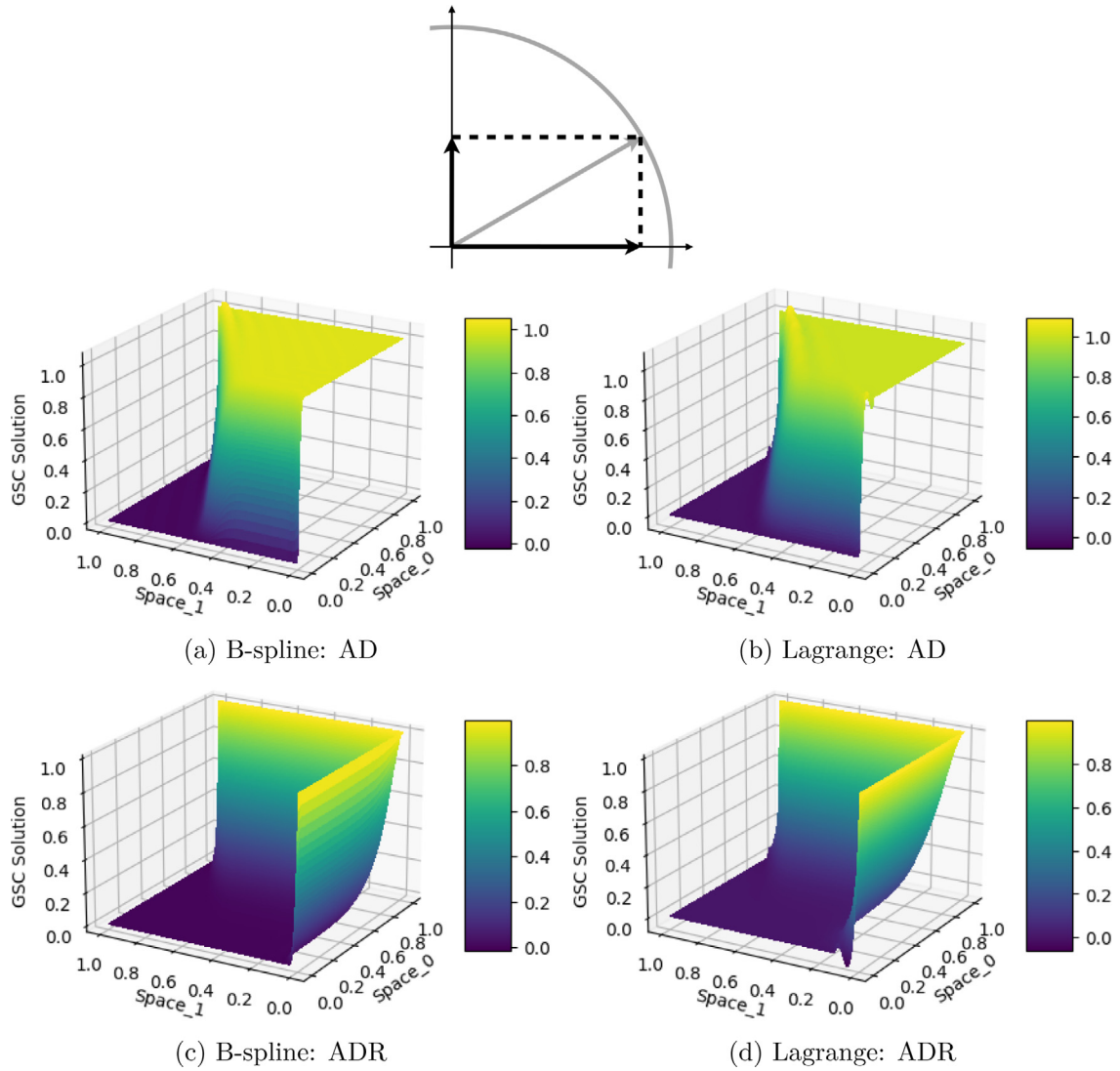


Fig. 6.3. Cubic approximate solutions computed with the directional GSC method for reactive rate $r = 7.5 \times 10^3 \text{ s}^{-1}$, advective velocity $\mathbf{a} = -1.0 \times 10^3 \text{ m s}^{-1} [\cos 30^\circ, \sin 30^\circ]$, and diffusivity $\kappa = 1.0 \text{ m}^2 \text{ s}^{-1}$.

matrices for the three methods from their corresponding bilinear forms with entries given by

$$\begin{aligned} \mathbf{M}_{AB} &= B^h(\omega_A, \omega_B) \\ \mathbf{M}_{AB}^{\text{DGSC}} &= \mathbf{M}_{AB} + (\tau_1 a_1 \partial_1 \omega_A + \tau_2 a_2 \partial_2 \omega_A, \mathbf{a} \cdot \nabla \omega_B - \kappa \Delta \omega_B)_{\tilde{\Omega}} \\ \mathbf{M}_{AB}^{\text{SGSC}} &= \mathbf{M}_{AB} + (\tau \mathbf{a} \cdot \nabla \omega_A, \mathbf{a} \cdot \nabla \omega_B - \kappa \Delta \omega_B)_{\tilde{\Omega}} \end{aligned}$$

where

$$\tau_i = \frac{h}{a_i} \left(\frac{1}{2} \coth(0.5 P e_h^i) - \frac{1}{P e_h^i} \right), \quad \tau = \frac{h}{\|\mathbf{a}\|_2} \left(\frac{1}{2} \coth(0.5 P e_h) - \frac{1}{P e_h} \right)$$

For all three methods above, we define the following common stability norm as a basis of comparison

$$\|v\|_{\text{Stab}}^2 := \left\| \kappa^{\frac{1}{2}} \nabla v \right\|_{\Omega}^2 + \left\| \tau^{\frac{1}{2}} \mathbf{a} \cdot \nabla v \right\|_{\Omega}^2 + \left\| \sigma_1^{\frac{1}{2}} a_1 \partial_1 v + \sigma_2^{\frac{1}{2}} a_2 \partial_2 v \right\|_{\Omega}^2,$$

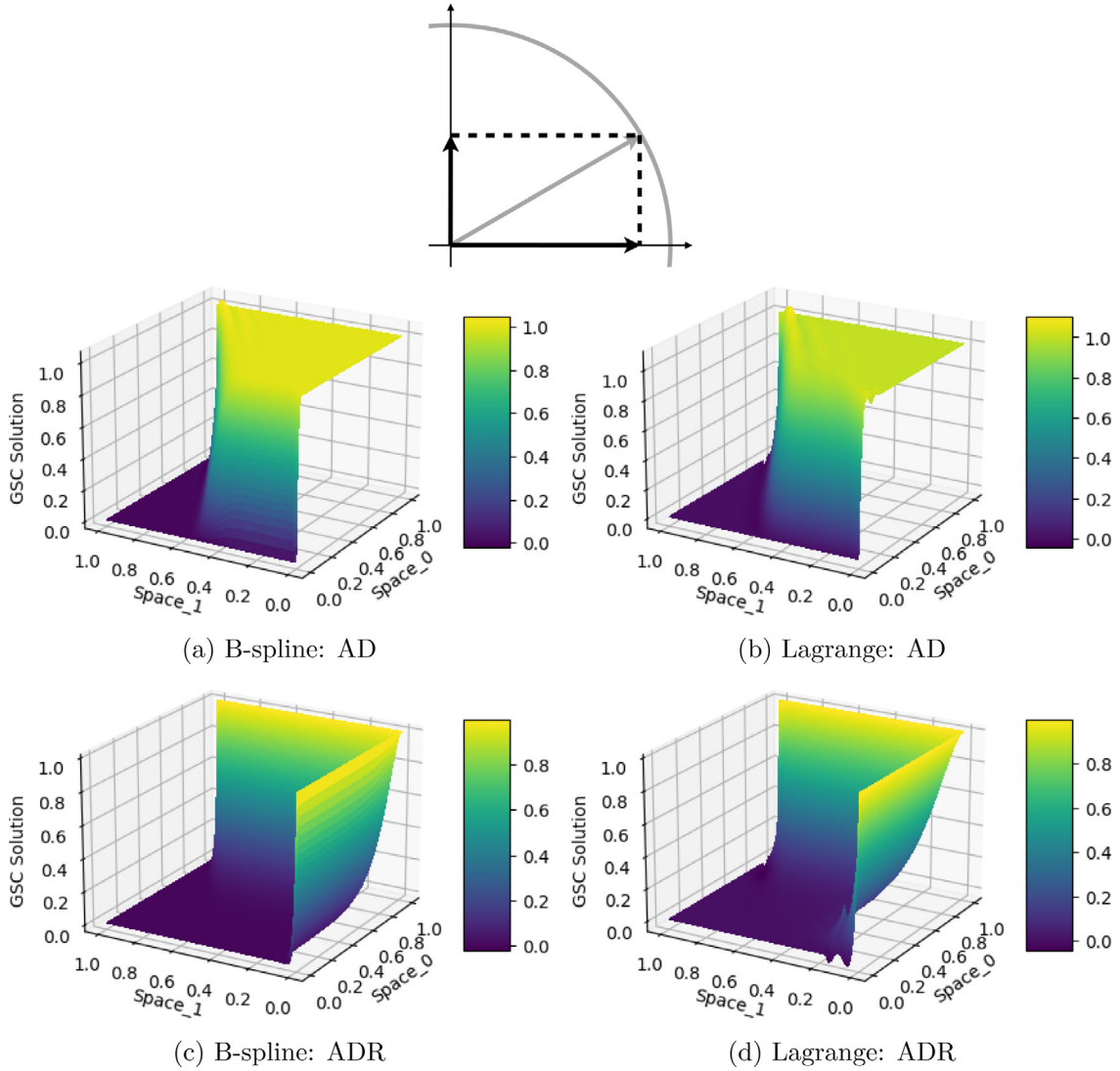


Fig. 6.4. Quartic approximate solutions computed with the directional GSC method for reactive rate $r = 7.5 \times 10^3 \text{ s}^{-1}$, advective velocity $\mathbf{a} = -1.0 \times 10^3 \text{ m s}^{-1} [\cos 30^\circ, \sin 30^\circ]$, and diffusivity $\kappa = 1.0 \text{ m}^2 \text{ s}^{-1}$.

where $\sigma_i = \frac{\tau_i^2}{\tau}$, from which we can define a corresponding matrix Θ with entries

$$\Theta_{AB} = (\kappa \nabla \omega_A, \nabla \omega_B) + (\tau \mathbf{a} \cdot \nabla \omega_A, \mathbf{a} \cdot \nabla \omega_B) + \left(\sigma_1^{\frac{1}{2}} a_1 \partial_1 \omega_A + \sigma_2^{\frac{1}{2}} a_2 \partial_2 \omega_A, \sigma_1^{\frac{1}{2}} a_1 \partial_1 \omega_B + \sigma_2^{\frac{1}{2}} a_2 \partial_2 \omega_B \right).$$

Given a discretization that leads to the matrices \mathbf{M} and Θ , one can show that the left-hand side of (35) is bounded below by the square root of the minimum eigenvalue, $\sqrt{\lambda_{\min}}$, to the problem

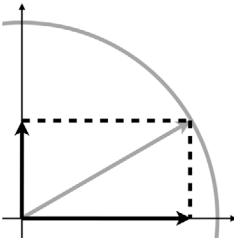
$$\left(\mathbf{M}^T \Theta^{-1} \mathbf{M} \right) \mathbf{z} = \lambda \Theta \mathbf{z}. \tag{37}$$

Furthermore, as the inequality (34) for all three methods can be proved with respect to the norm

$$\|v\|^2 := \left\| \kappa^{\frac{1}{2}} \nabla v \right\|_{\tilde{\Omega}}^2 + \left\| \tau^{-\frac{1}{2}} v \right\|_{\tilde{\Omega}}^2 + \left\| \tau^{\frac{1}{2}} \mathbf{a} \cdot \nabla v \right\|_{\tilde{\Omega}}^2 + \left\| \tau^{\frac{1}{2}} \kappa \Delta v \right\|_{\tilde{\Omega}}^2,$$

Table 6.2

Minimum and maximum values of the directional GSC solutions in Figs. 6.1, 6.2, 6.3, and 6.4. The corresponding values for the streamline GSC method are listed in Table 5.2.



Order	Basis	AD		ADR	
		min ·10 ⁻²	max	min ·10 ⁻²	max
Linear	B-spline/ Lagrange	-1.107	1.062	-6.910	1.000
Quadratic	B-spline	-2.351	1.060	-1.253	1.000
	Lagrange	-12.50	1.125	-12.50	1.000
Cubic	B-spline	-2.112	1.055	-1.373	1.000
	Lagrange	-6.413	1.093	-6.413	1.000
Quartic	B-spline	-1.971	1.048	-1.867	1.000
	Lagrange	-4.167	1.104	-4.167	1.000

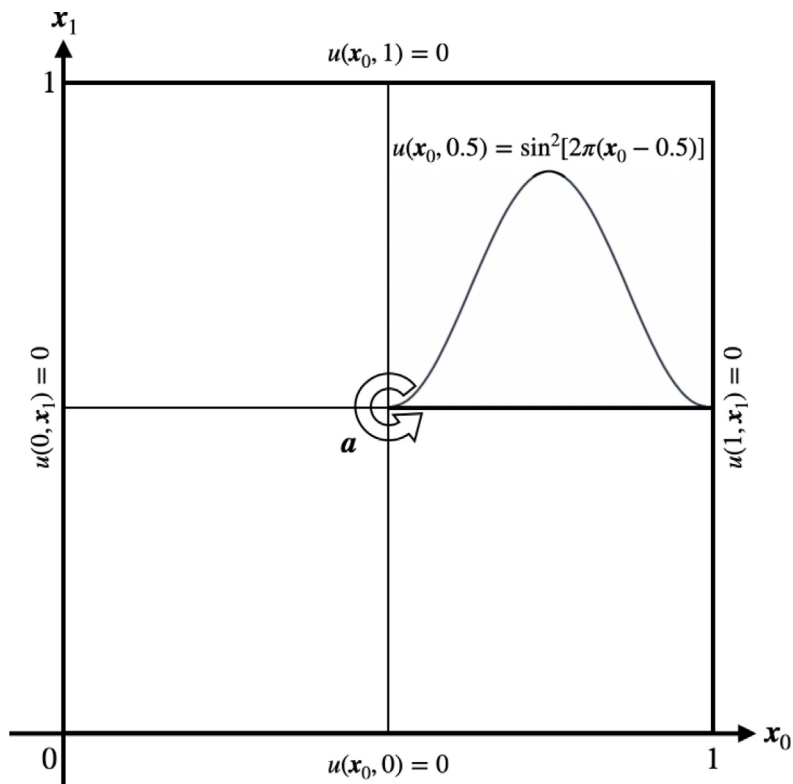


Fig. 6.5. Schematic of the “donut problem”.

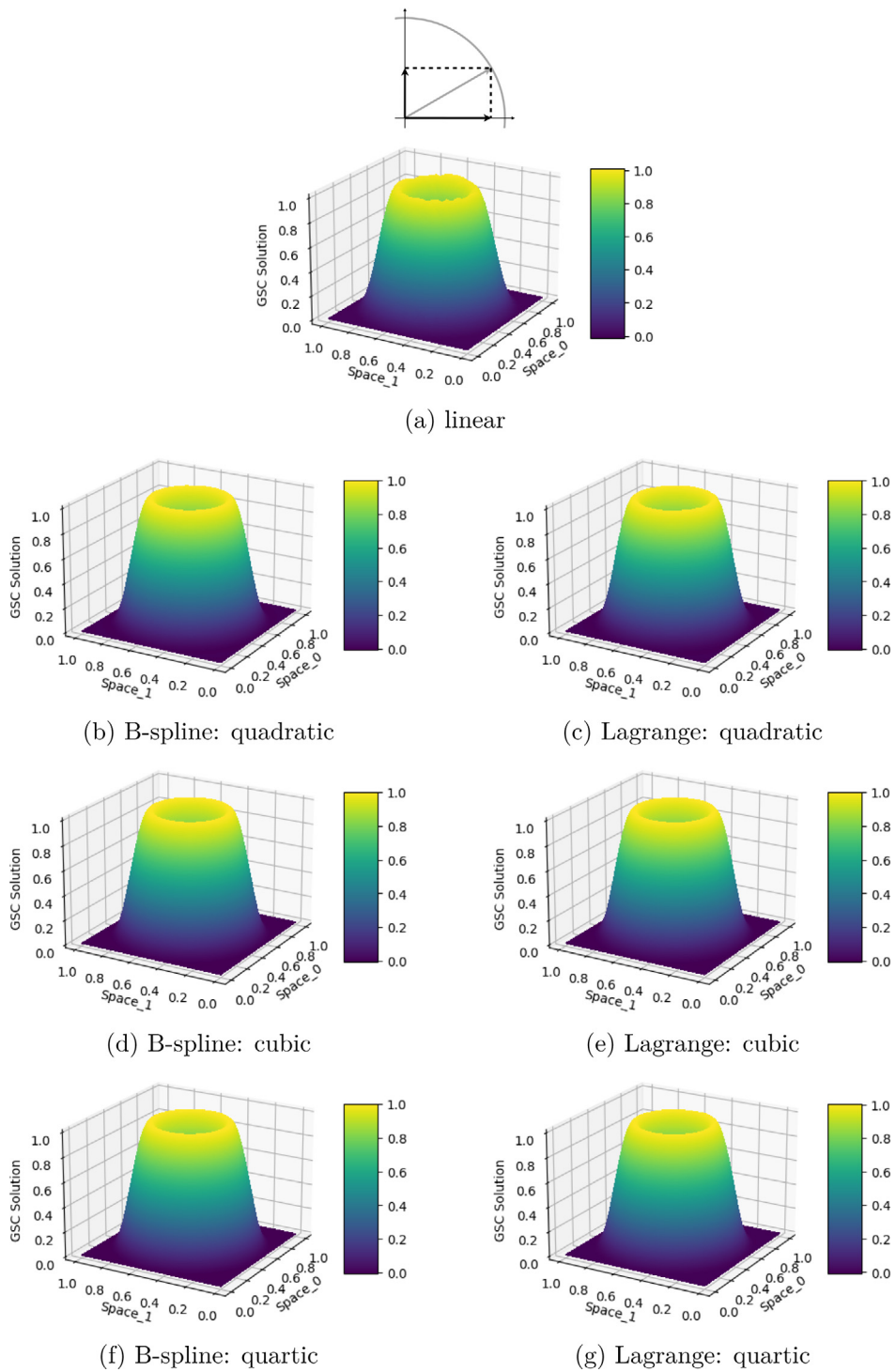


Fig. 6.6. Approximate solutions computed with B-spline and Lagrange basis functions of up to fourth order for the directional GSC method for advective velocity $\mathbf{a} = 1.0 \times 10^7 \text{ m s}^{-1} [0.5 - \mathbf{x}_1, \mathbf{x}_0 - 0.5]$ and diffusivity $\kappa = 1.0 \text{ m}^2 \text{ s}^{-1}$.

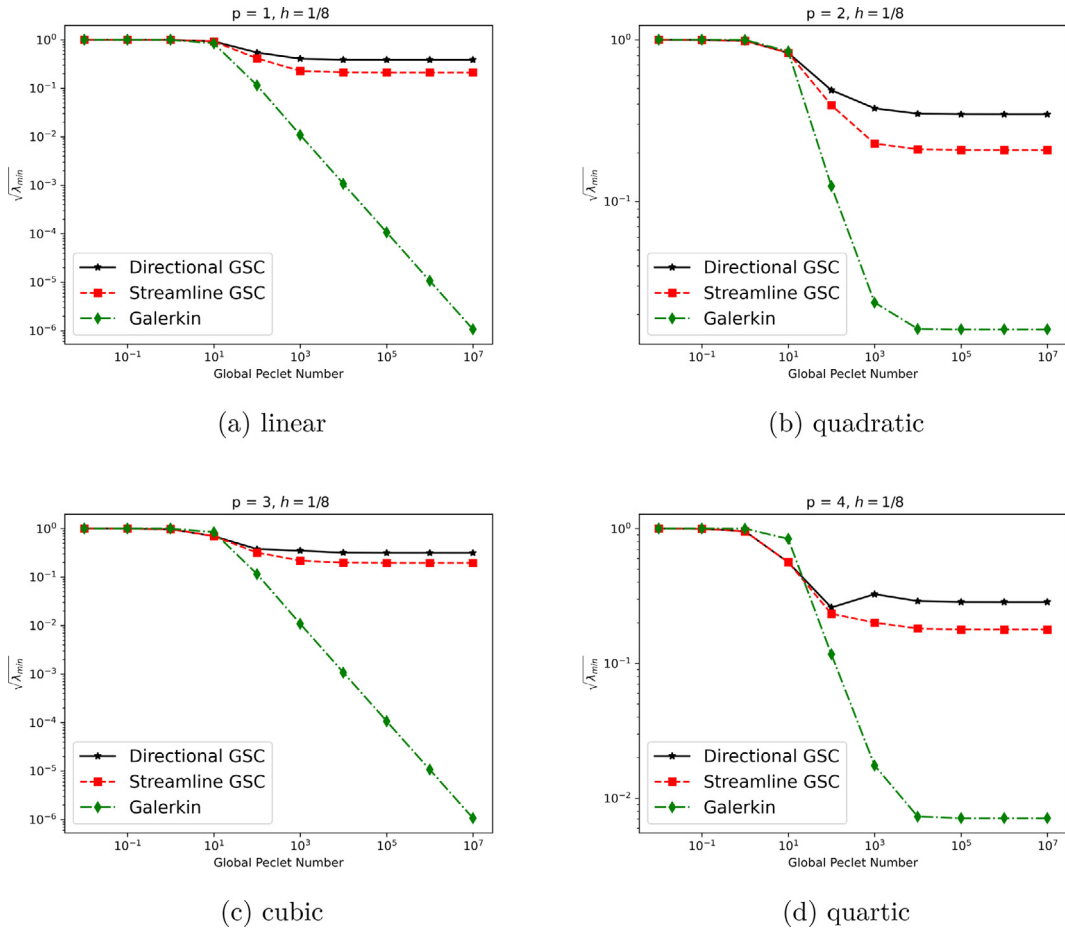


Fig. 6.7. We discretize the domain using B-splines ($h = \frac{1}{8}$) and calculate $\sqrt{\lambda_{\min}}$ from Eq. (37) for the directional GSC method, the streamline GSC method (i.e., SUPG), and the Galerkin method. We find that the directional and streamline GSC methods are stable whereas the Galerkin method is unstable as the global Péclet number is increased.

the inequality (36) shows that the larger the minimum eigenvalue obtained, the more stable the method.

For the test of stability, the problem setup is a variation of the Advection-Skew-to-Mesh problem (see Fig. 5.1). The advective velocity is fixed at $\mathbf{a} = (\cos(30^\circ), \sin(30^\circ))^T$ while diffusivity κ is allowed to vary in order to control the global Péclet number for the problem $Pe := \frac{\|\mathbf{a}\|_2}{\kappa} = \frac{Pe_h}{h}$. We use maximally smooth B-splines of order $p \in \{1, 2, 3, 4\}$ defined on a uniform mesh with element size h . The reason for using these is the slower degree-of-freedom growth rate during h - and p -refinement when compared to Lagrange elements. This is a very important consideration due to the computational cost of finding eigenvalues to Eq. (37).

We present two sets of results. In the first set, we fix the discretization ($h = \frac{1}{8}$) and look at the behavior of the minimum eigenvalue as the global Péclet number is increased. The results from linears up to quartic splines (see Fig. 6.7) consistently show that the directional GSC method and the streamline GSC method each yield a bound that remains relatively stable over a very large range of Pe with the directional GSC method yielding a slightly larger minimum eigenvalue than the streamline GSC method. The minimum eigenvalue of the Galerkin method tends to decrease with increasing Pe and ends up being at least an order of magnitude smaller than that of the stabilized methods. For splines of odd order, $\sqrt{\lambda_{\min}}$ in the Galerkin method appears to decrease monotonically, while for splines of even order, it eventually settles at a fixed value.

In the second set of results, we fix the global Péclet number ($Pe = 10^3$) and calculate $\sqrt{\lambda_{\min}}$ for decreasing element sizes h . The significant computational resources required only allowed us to perform this calculation for linear and quadratic splines. The results are depicted in Fig. 6.8. In both cases at larger h , we find that the directional

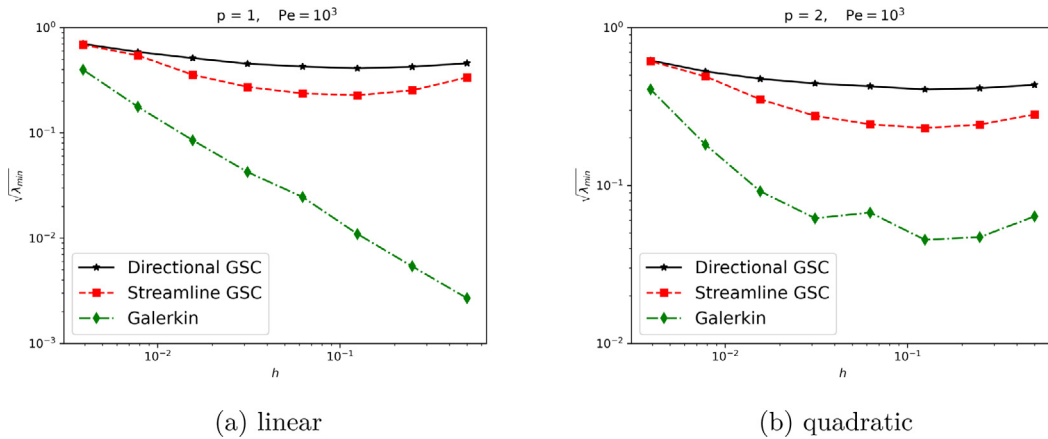


Fig. 6.8. We fix the global Péclet number at 10^3 and calculate the square root of the minimum eigenvalue $\sqrt{\lambda_{\min}}$ while successively refining the B-spline-based discretization of the domain. Initially, only the directional GSC and streamline GSC methods are stable whereas the Galerkin method is unstable. The Galerkin method stabilizes when the mesh is sufficiently refined.

and streamline GSC each produce a $\sqrt{\lambda_{\min}}$ that is at least an order of magnitude larger than that produced by the Galerkin method. Additionally, the directional and streamline GSC methods show relatively little change in $\sqrt{\lambda_{\min}}$ over the full range of refinements. That said, the directional GSC method gives a slightly larger value for the minimum eigenvalue than the streamline GSC method for larger values of h . As the mesh is refined ($h \rightarrow 0$), the minimum eigenvalue for all three methods converge. This is to be expected because as the element Péclet number Pe_h decreases, the need for stabilization disappears.

7. Conclusions

We have presented two new methods for solving the steady advection-diffusion-reaction (ADR) equation, the **Streamline GSC Method** and the **Directional GSC Method**. Both methods utilize stabilization concepts emanating from one-dimensional analysis of linear finite elements (linear B-splines) but their generalization to multidimensions differ. As the name suggests, the streamline GSC method employs SUPG stabilization for advection, but adds a gradient weighting of the reaction term times the gradient of the residual. The directional GSC method splits the weighting into one-dimensional advection and diffusion operators. We evaluated the methods numerically on a series of advection- and reaction-dominated problems for linear, quadratic, cubic, and quartic Lagrange and B-spline elements. The directional GSC method improves upon the deficiency of overshooting/undershooting in multidimensional boundary layer problems that has long been noted in SUPG and similar methods, especially for linear finite elements.

All the numerical results may be described as satisfactory but the B-spline elements consistently outperform the Lagrange elements when the same number of unknowns is used. For the streamline GSC method, we are able to prove (coercive) stability, convergence, and an optimal-order error estimate in the GSC norm. The error estimate is robust even for dominant advection and reaction due to the strength of the GSC norm. The directional GSC method is not coercive but we conjecture it is *inf-sup* stable. We support this with numerical computations of the *inf-sup* constant in a strong norm.

We think the GSC methods are a positive step in the solution of ADR problems. We are particularly encouraged by the performance of the directional GSC method. However, a functional analysis proof of stability is lacking. Another shortcoming is the reliance on the stabilization results of one-dimensional linear finite elements for higher-order cases. There are opportunities to improve upon this in several ways. First, an analysis of higher-order one-dimensional finite and B-spline elements is needed for the full ADR equation. This is a topic that we are very interested in and hope to pursue in future work. Second, the generalizations from one dimension to multiple dimensions is *ad hoc* and needs a more fundamental basis. This has been an open problem for many years. Third, although the boundary-layer overshooting/undershooting problem associated with flows at an angle to the boundary seems to be alleviated by the directional GSC method, there are still overshoots/undershoots at corners where

two boundaries come together. These arise all too often in practical engineering calculations. Finally, there is nothing in these methods that directly addresses the issue of monotonicity. This has been a difficult area for finite elements although, as can be seen, the present GSC methods perform well. Monotonicity and accuracy are competing attributes and finite elements and B-spline elements have had significant success with the latter, but not the former. However, in some applications, strict monotonicity is essential and there are very few finite element methods that achieve it; the elements are always very low-order, typically linear triangles, and the methods are always nonlinear. We refer the reader to the comprehensive and excellent recent review paper on this topic by Barrenechea, John, and Knobloch [23]. This is another important area of research.

Declaration of competing interest

The authors declare that they have no known competing financial interests or personal relationships that could have appeared to influence the work reported in this paper.

Data availability

No data was used for the research described in the article.

Acknowledgments

The support by the German Research Foundation (DFG) through project 33849990/GRK2379 (IRTG “Modern Inverse Problems”) is gratefully acknowledged.

Appendix A. Limits of stabilization parameters for vanishing reaction

To find the limits of the exact nondimensional stabilization parameters χ, ζ for vanishing reaction, i.e., $Da_h \rightarrow 0$, the series expansion

$$\begin{aligned} \cosh \sqrt{0.25Pe_h^2 + Da_h} &= \cosh(0.5Pe_h) + \\ &\frac{\sinh(0.5Pe_h)}{Pe_h} Da_h + \\ &\frac{Pe_h \cosh(0.5Pe_h) - \sinh(0.5Pe_h)}{2Pe_h^3} Da_h^2 + \\ &\frac{(Pe_h^2 + 12) \sinh(0.5Pe_h) - 6Pe_h \cosh(0.5Pe_h)}{6Pe_h^5} Da_h^3 + \\ &\mathcal{O}(Da_h^4), \end{aligned}$$

is substituted into their definitions in Eq. (22)

$$\zeta = \frac{Pe_h \left[\cosh \sqrt{0.25Pe_h^2 + Da_h} - \cosh(0.5Pe_h) \right] - Da_h \sinh(0.5Pe_h)}{Da_h \left[\cosh \sqrt{0.25Pe_h^2 + Da_h} - \cosh(0.5Pe_h) \right]}$$

and

$$\begin{aligned} \chi &= \frac{1}{6} + \frac{Da_h^2 \cosh(0.5Pe_h)}{2Da_h^2 \left[\cosh \sqrt{0.25Pe_h^2 + Da_h} - \cosh(0.5Pe_h) \right]} - \\ &\frac{(Da_h + Pe_h^2) \left[\cosh \sqrt{0.25Pe_h^2 + Da_h} - \cosh(0.5Pe_h) \right] - Da_h Pe_h \sinh(0.5Pe_h)}{Da_h^2 \left[\cosh \sqrt{0.25Pe_h^2 + Da_h} - \cosh(0.5Pe_h) \right]} \end{aligned}$$

to obtain

$$\zeta = \frac{[Pe_h \cosh(0.5Pe_h) - 2 \sinh(0.5Pe_h)] Da_h^2 + \mathcal{O}(Da_h^3)}{Pe_h \sinh(0.5Pe_h) Da_h^2 + \mathcal{O}(Da_h^3)}$$

$$\xrightarrow{Da_h \rightarrow 0} \frac{\coth(0.5Pe_h)}{2} - \frac{1}{Pe_h} = \zeta^{AD}$$

and

$$\chi = \frac{1}{6} - \frac{1 + \mathcal{O}(Da_h)}{6 + \mathcal{O}(Da_h)} - \frac{[\sinh(0.5Pe_h) - Pe_h \cosh(0.5Pe_h)] Da_h^3 + \mathcal{O}(Da_h^4)}{2Pe_h^2 \sinh(0.5Pe_h) Da_h^3 + \mathcal{O}(Da_h^4)}$$

$$\xrightarrow{Da_h \rightarrow 0} \frac{1}{Pe_h} \left[\frac{\coth(0.5Pe_h)}{2} - \frac{1}{Pe_h} \right] = \frac{\zeta^{AD}}{Pe_h}.$$

Note that the nondimensional advective stabilization parameter ζ converges to the well-known SUPG result for vanishing reaction r .

Appendix B. Principal axes of tensor-product elements in two dimensions

The principal axes $\tilde{\mathbf{e}}_j$ of tensor-product elements — that have the parametric domains $\tilde{\Omega}^e$ and are mapped to Euclidean space by endomorphisms \mathbf{x} — are given as the orthonormal eigenvectors of the symmetric-positive-definite inertia matrices

$$\tilde{\mathbf{I}} = \int_{\tilde{\Omega}^e} (\mathbf{x} - \bar{\mathbf{x}}^e) (\mathbf{x} - \bar{\mathbf{x}}^e)^T J^e d\xi,$$

where

$$\bar{\mathbf{x}}^e = \frac{1}{V^e} \int_{\tilde{\Omega}^e} \mathbf{x} J^e d\xi$$

are the elements' centroids,

$$V^e = \int_{\tilde{\Omega}^e} J^e d\xi$$

the elements' volumes and J^e the elements' Jacobian determinants. Coordinates $\tilde{\mathbf{a}}$ with respect to these principal axes can be transformed to the coordinates \mathbf{a} with respect to the Euclidean axes \mathbf{e}_i fulfilling

$$\tilde{\mathbf{e}}_j = \sum_i \mathbf{T}_i^{ij} \mathbf{e}_i$$

by means of the change-of-basis matrix \mathbf{T}_i :

$$\mathbf{a} = \mathbf{T}_i \tilde{\mathbf{a}}.$$

References

- [1] Isaac Harari, Thomas J.R. Hughes, Stabilized finite element methods for steady advection-diffusion with production, *Comput. Methods Appl. Mech. Eng.* 115 (1994) 165–191, [http://dx.doi.org/10.1016/0045-7825\(94\)90193-7](http://dx.doi.org/10.1016/0045-7825(94)90193-7).
- [2] Maria I. Asensio, Alessandro Russo, Giancarlo Sangalli, The residual-free bubble numerical method with quadratic elements, *Math. Models Methods Appl. Sci.* 14 (5) (2004) 641–661, <http://dx.doi.org/10.1142/S0218202504003398>.
- [3] Franco Brezzi, Donatella Marini, Augmented spaces, two-level methods, and stabilizing subgrids, *Int. J. Numer. Methods Fluids* 40 (1–2) (2002) 31–46, <http://dx.doi.org/10.1002/flid.265>.
- [4] Franco Brezzi, Leopoldo P. Franca, Thomas J.R. Hughes, Alessandro Russo, $b = f g$, *Comput. Methods Appl. Mech. Eng.* 145 (1997) 329–339, [http://dx.doi.org/10.1016/S0045-7825\(97\)87038-7](http://dx.doi.org/10.1016/S0045-7825(97)87038-7).
- [5] Franco Brezzi, Guillermo Hauke, Donatella Marini, Giancarlo Sangalli, Link-cutting bubbles for the stabilization of convection-diffusion-reaction problems, *Math. Models Methods Appl. Sci.* 13 (3) (2003) 445–461, <http://dx.doi.org/10.1142/S0218202503002581>.
- [6] Franco Brezzi, Donatella Marini, Alessandro Russo, On the choice of a stabilizing subgrid for convection-diffusion problems, *Comput. Methods Appl. Mech. Eng.* 194 (2005) 127–148, <http://dx.doi.org/10.1016/j.cma.2004.02.022>.

- [7] Ramon Codina, Comparison of some finite element methods for solving the diffusion-convection-reaction equation, *Comput. Methods Appl. Mech. Eng.* 156 (1998) 185–210, [http://dx.doi.org/10.1016/S0045-7825\(97\)00206-5](http://dx.doi.org/10.1016/S0045-7825(97)00206-5).
- [8] Leopoldo P. Franca, Eduardo G.D. Do Carmo, The Galerkin gradient least-squares method, *Comput. Methods Appl. Mech. Eng.* 74 (1989) 41–54, [http://dx.doi.org/10.1016/0045-7825\(89\)90085-6](http://dx.doi.org/10.1016/0045-7825(89)90085-6).
- [9] Leopoldo P. Franca, Charbel Farhat, Bubble functions prompt unusual stabilized finite element methods, *Comput. Methods Appl. Mech. Eng.* 123 (1995) 299–308, [http://dx.doi.org/10.1016/0045-7825\(94\)00721-X](http://dx.doi.org/10.1016/0045-7825(94)00721-X).
- [10] Leopoldo P. Franca, Frederic Valentin, On an improved unusual stabilized finite element method for the advective-reactive-diffusive equation, *Comput. Methods Appl. Mech. Eng.* 190 (2000) 1785–1800, [http://dx.doi.org/10.1016/S0045-7825\(00\)00190-0](http://dx.doi.org/10.1016/S0045-7825(00)00190-0).
- [11] Guillermo Hauke, A simple stabilized method for the advection-diffusion-reaction equation, *Comput. Methods Appl. Mech. Eng.* 191 (27–28) (2002) 2925–2947, [http://dx.doi.org/10.1016/S0045-7825\(02\)00217-7](http://dx.doi.org/10.1016/S0045-7825(02)00217-7).
- [12] Guillermo Hauke, Mohamed H. Doweidar, Exploring new subgrid scale stabilized methods for advection-diffusion-reaction, in: *ECCOMAS - European Congress on Computational Methods in Applied Sciences and Engineering*, 2004.
- [13] Guillermo Hauke, Antoni García-Olivares, Variational subgrid scale formulations for the advection–diffusion–reaction equation, *Comput. Methods Appl. Mech. Eng.* 190 (51–52) (2001) 6847–6865, [http://dx.doi.org/10.1016/S0045-7825\(01\)00262-6](http://dx.doi.org/10.1016/S0045-7825(01)00262-6), Erratum 191(27–28):3123–3124, 2002, 10.1016/S0045-7825(02)00233-5.
- [14] Sergio R. Idelsohn, Norberto M. Nigro, Mario A. Storti, Gustavo C. Buscaglia, A Petrov-Galerkin formulation for advection-reaction-diffusion problems, *Comput. Methods Appl. Mech. Eng.* 136 (1996) 27–46, [http://dx.doi.org/10.1016/0045-7825\(96\)01008-0](http://dx.doi.org/10.1016/0045-7825(96)01008-0).
- [15] Eugenio Oñate, Juan Miquel, Guillermo Hauke, Stabilized formulation for the advection-diffusion-absorption equation using finite calculus and linear finite elements, *Comput. Methods Appl. Mech. Eng.* 195 (2006) 3926–3946, <http://dx.doi.org/10.1016/j.cma.2005.07.020>.
- [16] Tayfun Tezduyar, Youngjin Park, Discontinuity capturing finite element formulations for nonlinear convection-diffusion-reactions, *Comput. Methods Appl. Mech. Eng.* 59 (1986) 307–325, [http://dx.doi.org/10.1016/0045-7825\(86\)90003-4](http://dx.doi.org/10.1016/0045-7825(86)90003-4).
- [17] Frederic Valentin, Leopoldo P. Franca, Combining stabilized finite element methods, 1995, URL <http://ccm.ucdenver.edu/reports/rep048.pdf>.
- [18] Guillermo Hauke, Giancarlo Sangalli, Mohamed H. Doweidar, Combining adjoint stabilized methods for the advection-diffusion-reaction problem, *Math. Models Methods Appl. Sci.* 17 (2) (2007) 305–326, <http://dx.doi.org/10.1142/S0218202507001929>.
- [19] Thomas J.R. Hughes, Giancarlo Sangalli, Variational multiscale analysis: the fine-scale green’s function, projection, optimization, localization, and stabilized methods, *SIAM J. Numer. Anal.* 45 (2007) 539–557, <http://dx.doi.org/10.1137/050645646>.
- [20] Alexander N. Brooks, Thomas J.R. Hughes, Streamline upwind/Petrov-Galerkin formulations for convection dominated flows with particular emphasis on the incompressible Navier-Stokes equations, *Comput. Methods Appl. Mech. Eng.* 32 (1982) 199–259, [http://dx.doi.org/10.1016/0045-7825\(82\)90071-8](http://dx.doi.org/10.1016/0045-7825(82)90071-8).
- [21] Joost S.B. van Zwieten, Gertjan J. van Zwieten, Wijnand Hoitinga, *Nutils 7.0*, 2022.
- [22] Klaus-Jürgen Bathe, Dena Hendriana, Franco Brezzi, Giancarlo Sangalli, Inf-sup testing of upwind methods, *Int. J. Numer. Methods Eng.* 48 (2000) 745–760, [http://dx.doi.org/10.1002/\(SICI\)1097-0207\(20000620\)48:5<745::AID-NME904>3.0.CO;2-E](http://dx.doi.org/10.1002/(SICI)1097-0207(20000620)48:5<745::AID-NME904>3.0.CO;2-E).
- [23] Gabriel R. Barrenechea, Volker John, Petr Knobloch, Finite element methods respecting the discrete maximum principle for convection-diffusion equations, 2022.